Periodicities of Polar Mesospheric Clouds Inferred from a Meteorological Analysis and Forecast System

Stevens, M.H., Space Science Division, Naval Research Laboratory, Washington, DC 20375

Lieberman, R.S. GATS Inc., Boulder, CO

Siskind, D.E. and McCormack, J.P., Space Science Division, Naval Research Laboratory, Washington, DC, 20375

Hervig, M.E., GATS Inc., Driggs, ID

Englert, C.R., Space Science Division, Naval Research Laboratory, Washington, DC, 20375

J. Geophys. Res.

Revised, 7 February 2017

Key Points

1) Solar temperature tides and the 2-day and 5-day planetary waves are quantified throughout the northern and southern PMC regions.
2) The impact of these periodicities on PMC frequency and ice water content are determined.
3) PMC results are compared directly to two independent satellite datasets.

Abstract. There is currently ambiguity in what controls polar mesospheric cloud (PMC) periodicities near 83 km altitude. This is primarily because satellite and ground-based datasets cannot resolve global mesospheric temperature variability over the diurnal cycle. To address this limitation, we employ a global meteorological analysis and forecast system that assimilates mesospheric satellite data with two significant advances. The first is that we use output at a more rapid one hourly cadence, allowing for a quantitative description of diurnal (24 h), semi-diurnal (12 h), and terdiurnal oscillations. The second is that the output drives a simple PMC parameterization which depends only on the local temperature, pressure and water vapor concentrations. Our study focuses on results from July 2009 in the northern hemisphere and January 2008 in the southern hemisphere. We find that the 24 h migrating temperature tide as well as the 12 h and 24 h nonmigrating tides dominate northern PMC oscillations whereas the 12 h and 24 h nonmigrating tides dominate southern oscillations. Monthly averaged amplitudes for each of these components are generally 2-6 K with the larger amplitudes at lower PMC latitudes (50°). The 2 day and 5 day planetary waves also contribute in both hemispheres, with monthly averaged amplitudes from 1-3 K although these amplitudes can be as high as 4-6 K on some days. Over length scales of ~1000 km and time scales of ~1 week, we find that local temperature oscillations adequately describe mid-latitude PMC observations.

1. Introduction

Polar mesospheric clouds (PMC) typically form near 83 km at high latitudes in the summertime. Often called noctilucent clouds (NLC) when observed from the ground, they can vary on time scales from hours [*e.g.* Rapp *et al*., 2002] to decades [*e.g.* Hervig and Siskind, 2006; Hervig and Stevens, 2014; Hervig *et al*., 2016a] and on spatial scales from kilometers [*e.g.* Dalin *et al*., 2010; Baumgarten *et al*., 2012] to thousands of kilometers [*e.g.* Karlsson *et al*., 2009; Gumbel and Karlsson, 2011]. Their extreme sensitivity to small temperature changes makes them potentially diagnostic of upper mesospheric changes on all of the above temporal and spatial scales [*e.g.* Pertsev *et al*., 2014], which is valuable since the Earth's upper mesosphere is notoriously difficult to access observationally. However, their very capacity for change often makes it difficult to isolate what process is in control.

The PMC periodicities quantified herein include those driven by migrating and nonmigrating temperature tides as well as 2 day and 5 day planetary waves. Other longer period planetary waves with smaller amplitudes (< 2 K) such as the 16 day wave are known to exist in the polar summer mesosphere but are not considered in this study. The relationship between all these periodicities as a function of latitude is currently not well understood. Their isolation and quantification with latitude would therefore be a significant advance in the study of the upper mesosphere in general and of PMC in particular. At mid-latitudes (50°-60°) where PMC can be observed by the naked eye, reported mean lidar temperatures are not below the frost point at 83 km [Gerding *et al*., 2007; Gerding *et al*., 2013a] so that oscillations about the mean are particularly important in their formation. But even the primary source of variability leading to mid-latitude PMC formation is disputed and poorly understood. In particular, it is unclear whether they are formed locally [*e.g.* Herron *et al*., 2007; Hultgren *et al*., 2011; Russell *et al*., 2014], whether they are transported from high latitudes [*e.g*. Gerding *et al*., 2013a; Gerding *et al*., 2013b] or whether a combination of both processes lead to their appearance [*e.g.* Nielsen *et al*., 2011].

To better understand the physical processes controlling PMC periodicities, this study uses output from the high-altitude NOGAPS-ALPHA (Navy Operational Global Atmospheric Prediction System – Advanced-Level Physics High-Altitude) forecast-assimilation system. We also use a simple model of bulk thermodynamic equilibrium [Hervig *et al*., 2009] to calculate PMC frequency and ice water content (IWC) from each grid point and time step of the NOGAPS-ALPHA output. By characterizing PMC in this way, we neglect all transport and assume that PMC formation is locally controlled by temperature oscillations. We compare our PMC results directly with observations to assess the validity of this assumption. Our ultimate goal is to better understand what contributes to PMC periodicities.

2. NOGAPS-ALPHA and PMC

Previous PMC studies with NOGAPS-ALPHA quantified variations due to the migrating diurnal (24 h) temperature tide [Stevens *et al*., 2010] and inter-hemispheric coupling [Siskind *et al*., 2011]. Those studies used the standard formulation of NOGAPS-ALPHA with a six hourly update cycle of the 3D-variational data assimilation component [Eckermann *et al*., 2009]. This cadence is too low to resolve atmospheric variability on sub-diurnal time scales, such as semi-diurnal (12 h) oscillations. Here we describe the use of a reconfigured version of NOGAPS-ALPHA to produce output at a higher cadence. Our approach isolates both migrating solar tides, which are sun synchronous, and non-migrating tides, which are not. We describe our analysis of migrating temperature tides as well as their impact on PMC in Section 3 and for nonmigrating tides and planetary waves in Section 4.

2a. One Hourly NOGAPS-ALPHA Forecast Output

NOGAPS-ALPHA was developed as a prototype vertical extension of the Navy's operational forecast model to ~95-100 km. This vertical extension required inclusion of radiative heating and cooling rates that account for non-local thermodynamic equilibrium, ozone and water vapor transport and photochemistry, as well as non-orographic gravity wave drag [Hoppel *et al*., 2008; Eckermann *et al*., 2009]. The data assimilation component of NOGAPS-ALPHA assimilates conventional meteorological and temperature data from the Microwave Limb Sounder (MLS, Version 2.2) on the Aura satellite and the Sounding of the Atmosphere using Broadband Emission Radiometry (SABER, Version 1.07) instrument on the NASA TIMED satellite as well as MLS ozone and water vapor up to 90 km. In its original configuration, output for the analysis was calculated four times daily (six hourly cadence) and globally. The spatial resolution was 2° latitude × 2° longitude horizontally and 68 levels from the tropopause to the mesopause vertically.

As noted above, this six hourly cadence can alias higher order tidal modes. Therefore, the forecast model component NOGAPS-ALPHA was configured to be initialized by the assimilation every six hours and to produce forecast output on a one hourly cadence [Siskind *et al.* 2012; 2014; Siskind and Drob, 2014; Lieberman *et al*., 2015; Pancheva *et al*., 2016]. This provides better resolution of semi-diurnal migrating and nonmigrating tidal components, as reported by Lieberman *et al*. [2015]. Hourly output for temperature, geopotential height and horizontal winds are available for all of 2009 and for the 2007-2008, 2008-2009 and 2009-2010 southern summers. Since we focus on the formation and variation of PMC in the summertime, much of the emphasis of our study is on monthly averages of these fields in July 2009 (northern hemisphere summer) and January 2008 (southern hemisphere summer) as representative time periods to characterize the different components to PMC formation. The solar activity for these months was low with an average $F_{10.7}$ solar radio flux index of between 68-74 $\times 10^{-22}$ W/m^2/Hz. We consider other time periods as available and appropriate.

It is important to note that for water vapor, one hourly output was not archived. We thus rely on the standard six hourly water vapor output interpolated onto an hourly grid. We expect that the local water vapor mixing ratio varies inversely with the clouds as they form and sublimate [Rapp and Thomas, 2006]. However, we focus here on IWC variations, which is the vertically integrated ice mass density and more sensitive to temperature variations than water vapor variations [Hervig *et al*., 2015].

The calculation of PMC frequency and IWC from NOGAPS-ALPHA requires accurate vertical profiles of both temperature and water vapor. Small biases in temperature of a few Kelvin can have a significant effect on IWC. Recently the Solar Occultation For Ice Experiment (SOFIE) on NASA's Aeronomy of Ice in the Mesosphere (AIM) mission released a new dataset (Version 1.3) which corrected a known warm bias in upper mesospheric SOFIE temperatures [Stevens *et al*., 2012] so that they are now more consistent with several other datasets. This improvement to the SOFIE temperature product resulted from a better representation of atomic oxygen and carbon dioxide in the upper mesosphere [Hervig *et al*., 2016b]. We use these v1.3 temperatures as the standard with which to compare NOGAPS-ALPHA temperatures.

In order to directly compare NOGAPS-ALPHA one hourly temperature results with observations, we regrid the output from geopotential to geometric altitudes [Eckermann *et al*., 2009; Stull, 2000]. We then compare analyzed temperatures to SOFIE temperatures for the same latitude and local time (LT) as the SOFIE observations. Figure 1a shows the comparison of NOGAPS-ALPHA one hourly temperatures with SOFIE temperatures averaged over July 2009, where we have assembled the NOGAPS-ALPHA average at 68° N and between 23.0 and 23.4 LT to be consistent with the sampling of SOFIE. Over the month of July 2009, the comparison therefore averages 403 SOFIE profiles and 2232 NOGAPS-ALPHA profiles. Figure 1b shows the difference between the two and reveals that NOGAPS-ALPHA temperatures are 6 K lower than SOFIE v1.3 temperatures at 83 km. Although near the SOFIE mesopause there is almost no difference, NOGAPS-ALPHA temperatures are 10 K lower than SOFIE temperatures at 90 km.

Based on Figure 1, we infer that there is a temperature bias in the NOGAPS-ALPHA profiles and adjust them at all grid points throughout July 2009 with the difference shown in Figure 1b in order to be consistent with the SOFIE observations at 68° N. In this work, we do not use the analysis poleward of 80° latitude since these regions are essentially an extrapolation beyond where MLS and SABER observe. The upward 6 K adjustment to the NOGAPS-ALPHA temperatures at PMC altitudes is comparable to the combined systematic uncertainties estimated from the assimilated SABER (7 K) and MLS (2 K) temperature measurements in the polar summer mesosphere [Remsberg *et al*., 2008; Schwartz *et al*., 2008; Eckermann *et al*., 2009]. We also note that systematic temperature uncertainties in the polar summer for the SOFIE observations are estimated to be 2 K at PMC altitudes [Stevens *et al*., 2012] for v1.3 data.

This temperature adjustment is quantitatively similar to those performed by Hervig *et al*. [2016a] in an investigation using NOGAPS-ALPHA in PMC simulations of decadal variability. Analogous to the approach of Hervig *et al*., the NOGAPS-ALPHA temperature adjustments are identical for all profiles for each time period studied so that the relative temperature variability at a given altitude is not impacted. The adjustment affects the modeled PMC frequency and IWC, giving much better agreement with SOFIE observations.

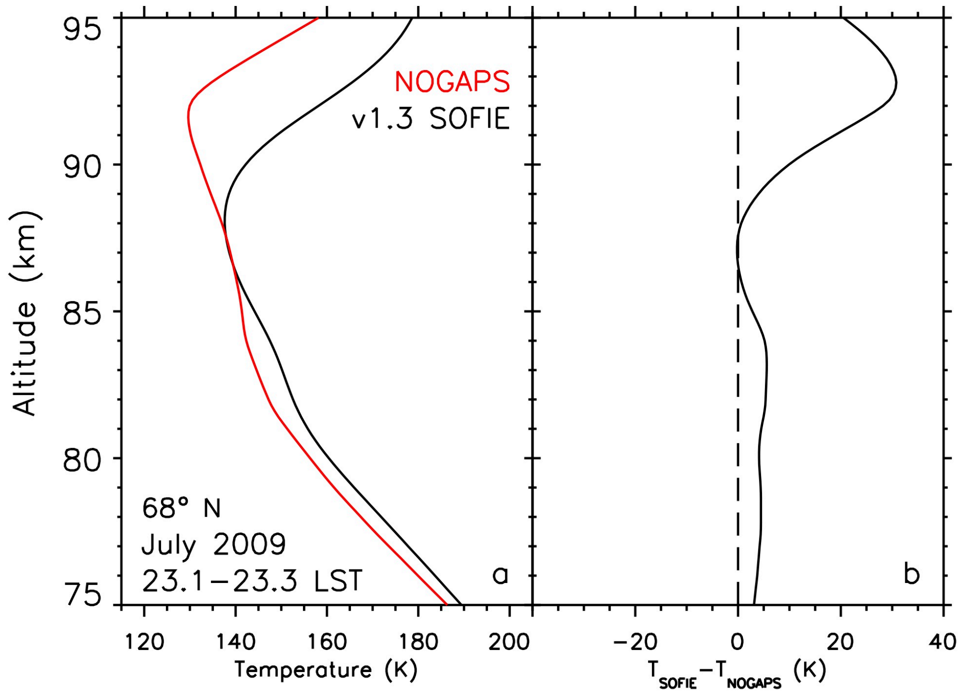

Figure 1. (a) SOFIE averaged temperatures for July 2009 (black) compared against NOGAPS-ALPHA hourly temperatures for the same latitude and LT of the SOFIE observations (red), as indicated. (b) The difference between the two profiles in Figure 1a.

After applying the adjustment to the NOGAPS-ALPHA hourly temperatures, we show Hovmöller plots for July 2009 in Figures 2a and 2b for 83 km geometric altitude at two different latitudes: 68° N and 55° N. This altitude is typical for northern hemisphere PMC and the latitudes are chosen to represent two important regions of formation considered. Figures 2a and 2b show the highly variable upper mesospheric temperatures throughout the month. This variability could be driven by tides, planetary waves and gravity waves. We will determine the relative contribution of tidal oscillations to these temperatures using monthly averages as discussed in Section 3. Diagonal westward propagating bands can be seen in the figures with periods longer than a day due to planetary waves [Merkel *et al*., 2008; Hultgren *et al*., 2011; Nielsen *et al*., 2011; Dalin *et al*., 2011]. McCormack *et al*. [2014] analyzed the monthly averaged contribution to this variability from planetary waves using the six-hourly NOGAPS-ALPHA product and the results of this analysis will be discussed further in Section 4.

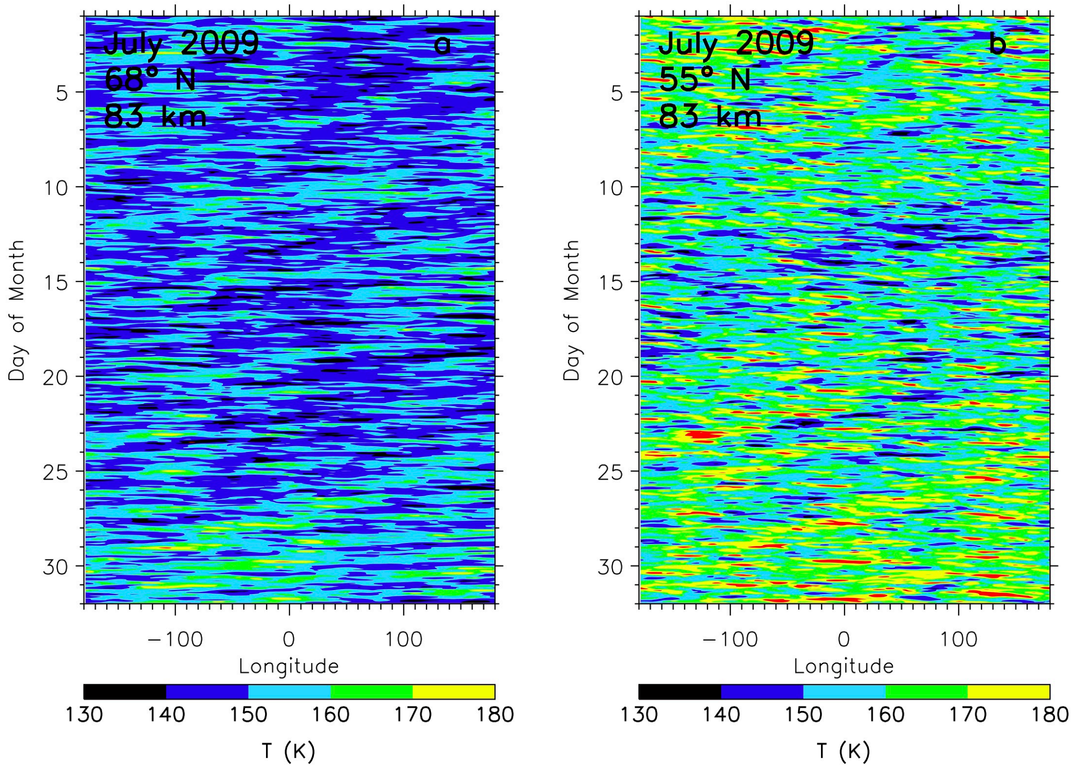

Figure 2. (a) Hovmöller plot showing temperatures for 83 km geometric altitude at 68° N during the month of July 2009. (b) Same except for 55° N. Red areas are where temperatures are in excess of 180 K.

2b. Calculating Local PMC Formation

Hervig *et al*. [2009] showed that PMC IWC can be calculated using only the assumption of bulk thermodynamic equilibrium and measured temperature, pressure and water vapor profiles. They furthermore showed that this IWC is in agreement with zonally averaged IWC observed by SOFIE to within 35%, indicating that vertical and horizontal transport of PMC can be neglected when calculating IWC at SOFIE latitudes. The model has been successfully used in a variety of PMC studies at high and mid-latitudes [Russell *et al*., 2010; 2014; Rong *et al*., 2012;

2014; Hervig *et al*., 2015; 2016b]. We will discuss our assumption of local PMC formation when comparing our PMC calculations against observations later in this study.

We show Hovmöller plots of calculated IWC for July 2009 in Figures 3a and 3b for the same two latitudes shown in Figures 2a and 2b. Since IWC is a vertically integrated quantity, the images show the total amount of mesospheric water ice present throughout each day and for each longitude. Although sensitive to temperature variations, IWC requires that the temperature be low enough to form a PMC, so Figure 3 is useful in assessing how the temperature oscillations in Figure 2 convey to PMC oscillations. In Figure 3a (68° N) the temperatures are low enough to produce ample PMC so that the temperature oscillations in Figure 2a are reflected in the IWC. In Figure 3b (55° N) PMC are far sparser, but the trough of the 5 day planetary wave shown in Figure 2b in the middle of the month is seen in the IWC image. SHIMMER PMC detections from the first half of the month are overplotted on Figure 3b and are close to where the IWC is highest, providing some validation of the IWC calculations. Figure 3b shows that the SHIMMER PMC and the calculated IWC qualitatively both show maxima between 12-15 July and 0-100° E, but there is not exact correspondence in space and time between the two. This could be due to the simple assumption of bulk thermodynamic equilibrium at every grid point for the calculated IWC, which may be less accurate when planetary waves are dominating PMC formation. The SHIMMER observations are discussed further in Section 3.

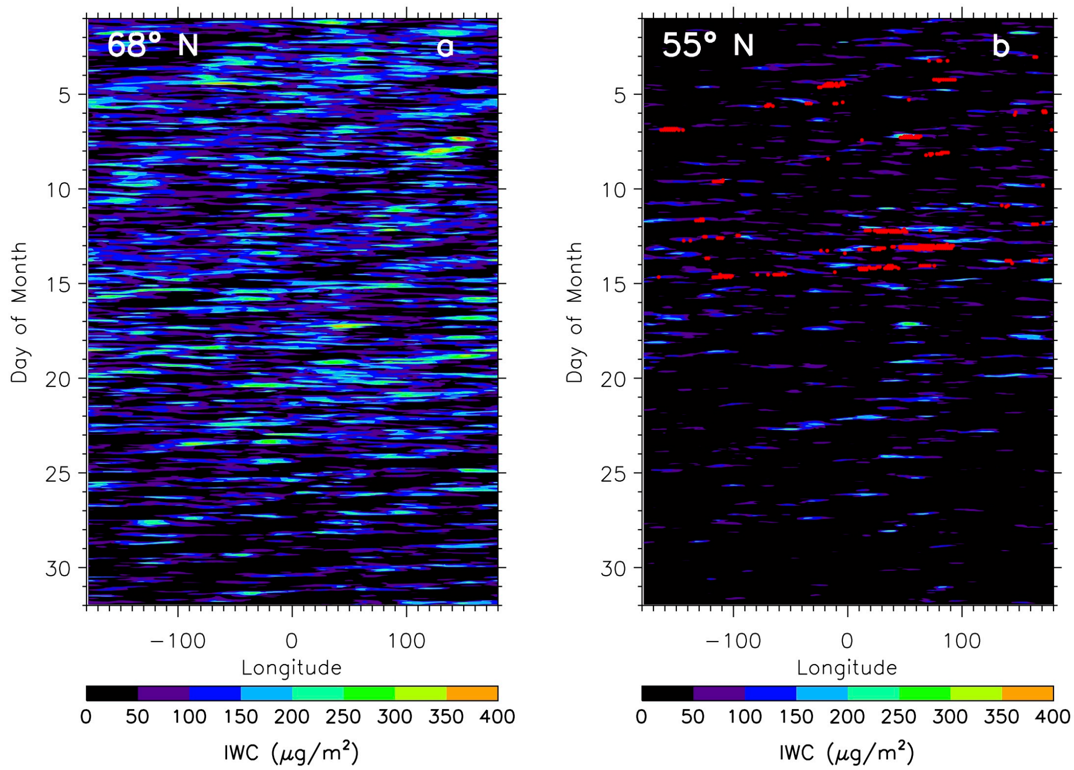

Figure 3. (a) Hovmöller plot of calculated IWC for 68° N in July 2009. Red areas are where IWC is in excess of 300 μg/m^2. (b) Same except that IWC is shown at 55° N. Note change in color scale. Red symbols indicate where SHIMMER observed PMC from 3-14 July and between 50-58° N.

3. Migrating Temperature Tides and PMC Oscillations

In this section we focus on migrating temperature tides and comparing PMC results to independent observations. Previous work by Stevens *et al*. [2010] used monthly averaged NOGAPS-ALPHA six hourly output on a LT grid to drive a microphysical model and quantify the evolution of mesospheric ice particles over the diurnal cycle. In contrast, we herein use the one hourly output and the simpler cloud parameterization described above to describe IWC at every spatial grid point and time step. This approach not only allows us to quantify the effects of both 24 h and 12 h migrating temperature tides on PMC but also allows us to separately derive periodicities of PMC frequency and IWC.

For PMC validation in this work we use datasets obtained at the same time as our analyses whenever possible. For comparison against PMC observations at high latitudes (~68°) we use concurrent SOFIE data. At mid-latitudes (50-58°) we use concurrent PMC frequencies observed by the Spatial Heterodyne Imager for Mesospheric Radicals (SHIMMER) on STPSat-1 [Englert *et al*., 2010; Stevens *et al*., 2010]. To calculate PMC frequency, we identify all NOGAPS-ALPHA grid points where the model shows PMC and compare that to all grid points in the analysis for each latitude.

3a. Northern Hemisphere: July 2009

Figure 4 shows the average variation of temperature over the diurnal cycle during July 2009 at 83 km geometric altitude for four different latitudes at which PMC can exist: 55° N, 60° N, 68° N and 80° N. There are several important aspects of these temperature results. First, the 24 h migrating temperature tide clearly dominates with an amplitude of 4-5 K between 55-68° N. This is consistent with previous studies using the six-hourly product for the northern summer in 2007-2009 [Stevens *et al*., 2010; McCormack *et al*., 2014]. Second, despite the faster cadence of the hourly product there is no evidence at any of the latitudes shown that the semi-diurnal migrating tide is more important than the diurnal migrating tide. Third, at 80° N the temperature oscillation over the diurnal cycle is very weak.

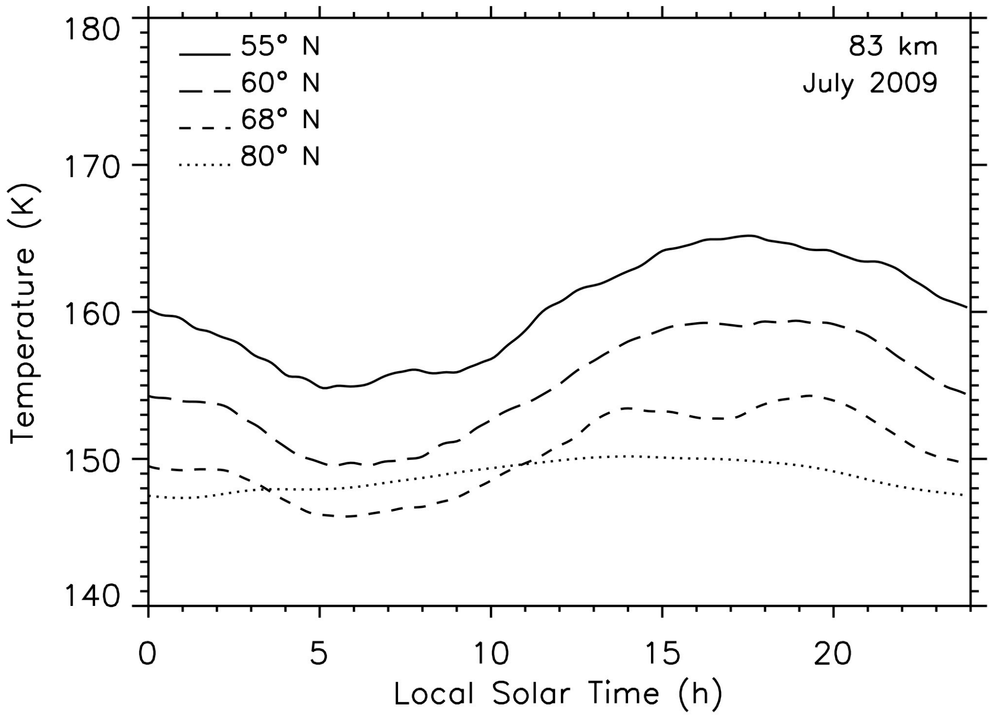

Figure 4. Average temperatures at 83 km over the diurnal cycle for July 2009 from the NOGAPS-ALPHA hourly product. Results at four different latitudes at which PMC can exist are shown.

Following the approach of Fiedler *et al*. [2011], we extract both diurnal and semi-diurnal temperature oscillations shown in Figure 4 with harmonics using a least-squares fitting procedure. Figure 5a shows the monthly zonal mean temperatures with latitude for July 2009, which range from 149 K at 80° N to 165 K at 50° N. Figures 5b and 5c show the amplitude and LT for the peaks of the 24 h and 12 h migrating temperature tide at each latitude. The 24 h amplitude peaks at 5 K near 60° N, then steadily decreases to about 1 K near 80° N whereas the 12 h amplitude is smaller than 1 K at all latitudes shown. The peak of the 24 h oscillation is consistently between 14-19 LT at all latitudes shown. Previous work by Zhang *et al.* [2006] using satellite data indicate that the 12 h amplitude is comparable to the 24 h amplitude at mid-latitudes, although their study does not extend to the PMC region poleward of 50° N.

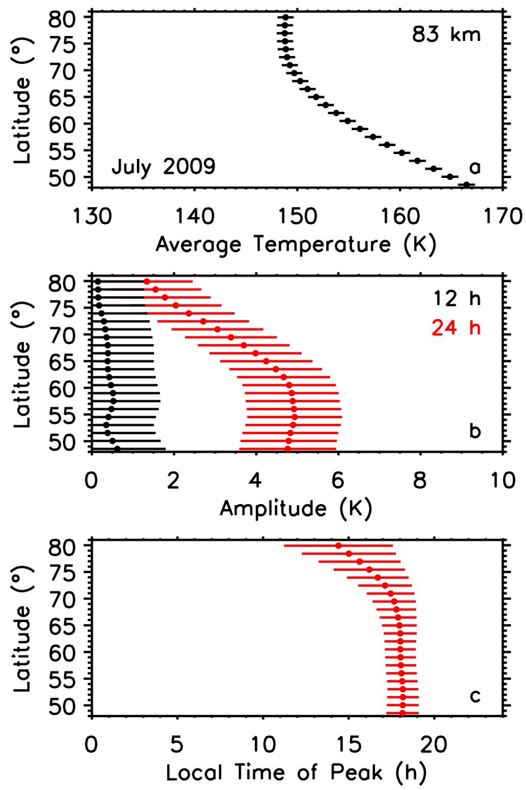

Figure 5. (a) Average temperatures at 83 km from the NOGAPS-ALPHA hourly product for July 2009 at 83 km. (b) Amplitudes of the migrating 24 h (red) and 12 h (black) temperature tide based on harmonic fits to the temperature. (c) Local time of the peak for the 24 h migrating tide. The semi-diurnal amplitude is small so its peak time is not shown.

Independent calculations of both PMC frequency and IWC enable a more direct comparison with existing PMC datasets. This approach also allows us to sort the derived PMC properties based on an instrument IWC threshold. Although SOFIE is sensitive enough to measure virtually all PMC, other instruments sample different latitudes and LT and are less sensitive so that direct comparison with these datasets requires us to use a higher IWC threshold. This subset of "stronger" PMC can have a much different behavior over latitude and over the diurnal cycle [Fiedler *et al*., 2005; Fiedler *et al*., 2011; DeLand *et al*., 2011]. There has been significant interest in the Solar Backscatter Ultraviolet (SBUV) suite of instruments, which has collected over 35-years of PMC data and represents the longest satellite dataset on record [*e.g.*

DeLand and Thomas, 2015; Hervig *et al*., 2016a]. Hervig and Stevens [2014] determined a threshold for the SBUV PMC detections of 40 μg/m^2 and we use that to identify a diagnostic IWC subset for comparison.

Figure 6a shows the calculated IWC over the diurnal cycle for all PMC in July 2009 at the same four latitudes shown in Figure 4. The IWC is calculated only where there is a PMC so that null detections are not averaged into the result in Figure 6a. As expected, the IWC is largest at the highest latitude and yields an IWC peak between 5-7 LT equatorward of 80° N. The IWC is 24% higher than that observed by SOFIE for the same viewing conditions. Figure 6b is the same as Figure 6a except that we only show the diurnal variation for the strong PMC (IWC > 40 μg/m^2). Diurnally averaged values are near 100 μg/m^2 and consistent with those previously reported for SBUV [Stevens *et al*., 2005; Hervig and Stevens, 2014; DeLand and Thomas, 2015].

We show calculated PMC frequencies in Figure 6c over the diurnal cycle for the same latitudes. Near 68° N the frequency is 85% at 23.2 LT and slightly less than that reported from SOFIE observations during the same month and year (90%). PMC frequency is near 100% at 80° N and therefore has virtually no variation throughout the diurnal cycle. Figure 6d shows the variation of PMC frequency over the diurnal cycle for strong PMC. Note that due to the higher temperatures at mid-latitudes there are much fewer strong PMC, which nearly disappear in the warm part of the day leading to a larger relative diurnal variation [Stevens *et al*., 2010; Fiedler *et al*., 2011].

While the phase of the diurnal cycle seen in Figure 6 (morning peak, late afternoon minimum) agrees with earlier results shown by Stevens *et al*. [2010], we note that the amplitude of the diurnal cycle shown in Figure 6 is smaller. For June 2007 at 69° N Stevens *et al*. [2010] found about a factor of six frequency weighted IWC variation, about twice what we infer here by combining the IWC and frequency in Figures 6a and 6c. We expect some differences due to the contrasting approaches that were used. While our earlier work used zonally and monthly averaged temperatures to describe PMC formation, in this work we define PMC properties at each time step and grid point. Moreover, we focus on a different month and year than the Stevens *et al*. [2010] results, which introduces different ambient temperatures in the PMC calculation and affects the relative PMC variation over the diurnal cycle.

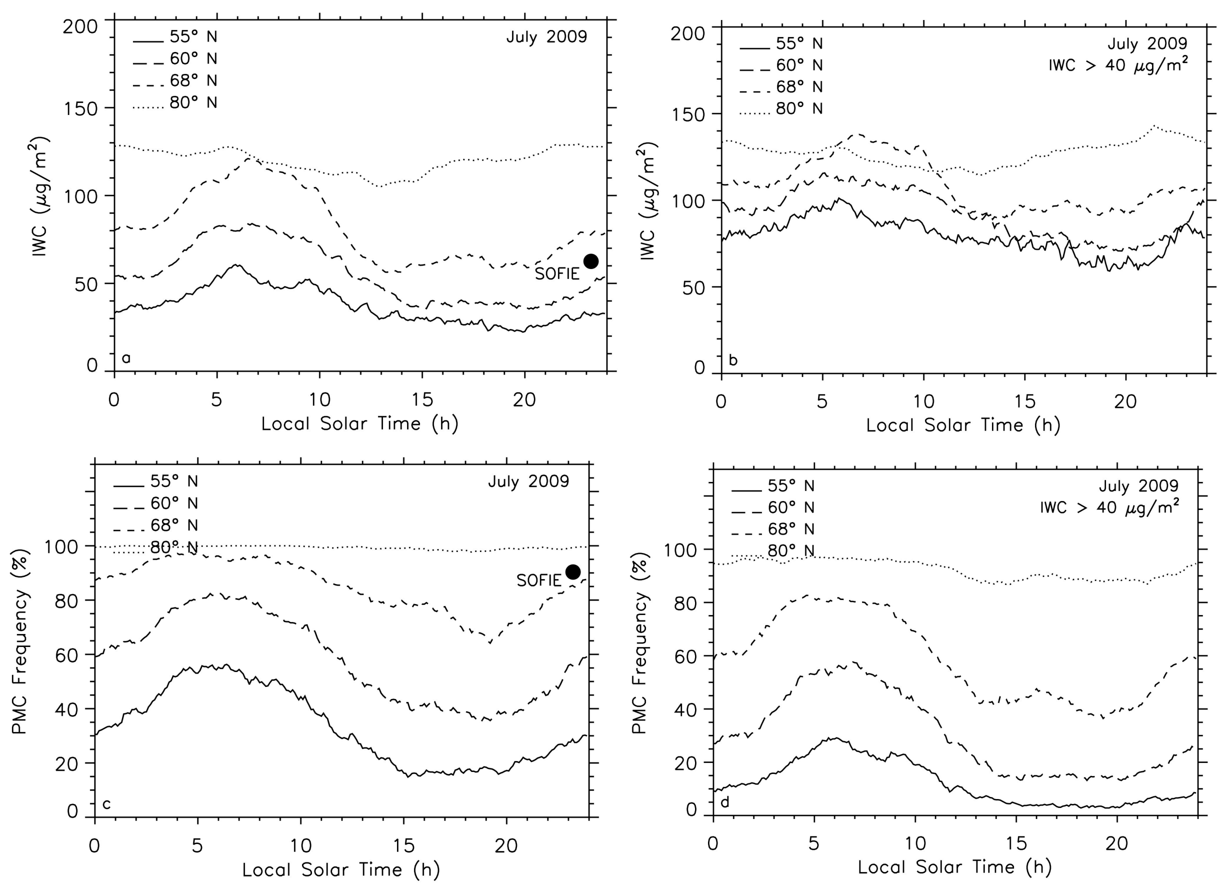

Figure 6. (a) Calculated IWC diurnal variation from the NOGAPS-ALPHA hourly product in July 2009 at four latitudes where PMC form. The IWC peak between 5-7 LT is due to the temperature minimum at the same time in Figure 4. The IWC is not weighted by frequency and the monthly averaged SOFIE IWC (at 68° N) is indicated(b) IWC from the same analysis but for "strong" PMC (IWC >40 μg/m^2). (c) Calculated diurnal variation of PMC frequency at the same four latitudes. The monthly averaged SOFIE frequency is indicated. (d) Same as Figure 6c except for strong PMC. Note that due to the longitudinal variability of temperature there are PMC throughout the diurnal cycle, even at 55° N.

Ground-based PMC data are not subject to the orbital constraints of satellite data and are therefore useful for comparison against LT variations. Using lidar data at 69° N averaged between 1997-2010, Fiedler *et al*. [2011] showed a peak frequency of 63% near 4.5 LT decreasing to a minimum of about 32% at 11.5 LT. In Figure 6d at 68° N the PMC frequency peaks near 83% at 4.5 LT and decreases to about 43% at 13 LT, which is remarkably similar to the Fiedler *et al*. results. We furthermore note that Fiedler *et al*. report a second smaller peak near 16 LT, which is also reproduced at 68° N in Figure 6d. Overall our results are in good agreement with the ground-based climatology given that the threshold used is not optimized for ground-based data.

At mid-latitudes, SHIMMER observed PMC between 50-58° N concurrent with our analysis in July 2009. SHIMMER observed throughout the daytime portion of the diurnal cycle so it is important to interpolate the latitude, longitude and LT of each SHIMMER image to the one hourly analysis. This approach was used by Russell *et al*. [2014] when comparing SHIMMER observations to derived PMC properties using the six hourly analysis. We repeat the approach of Russell *et al*. but with the one hourly product and with the archived SHIMMER data (ftp://spdf.gsfc.nasa.gov/pub/data/shimmer/), from which we derive PMC frequencies in Figure 7. We use a threshold for peak ice mass density of 30 ng/m^3 from which IWC is calculated, which is slightly lower than the best estimate of Russell *et al*. [2014] in their independent analysis of the SHIMMER data (40 ng/m^3). We note however that our approach differs slightly from Russell *et al*. in a few aspects. First of all, we have adjusted the NOGAPS-ALPHA temperatures upward (see Figure 1) to agree with the SOFIE (v1.3) observations at higher latitudes. Secondly, we use the one hourly NOGAPS-ALPHA results rather than the six hourly results. Finally, we note that we focus on less than a month of SHIMMER data for analysis rather than the entire 3 year dataset. We have omitted the second half of July 2009 in Figure 7 due to limited operations and sparse coverage by SHIMMER.

Figure 7 shows that the LT for the SHIMMER observations start near noon at the beginning of the month and decrease by about 30 min per day. The modeled peak frequency in the middle of the month is driven by both a particularly deep trough in the 5 day planetary wave (Figures 2b and 3b) and the migrating 24 h temperature tide, which has a minimum near 6 LT when SHIMMER was observing in mid-July. The combined effects of these two mid-latitude components during this same time period were discussed by Hultgren *et al.* [2011]. Other components such as the 16 day planetary wave [*e.g.* Kirkwood and Stebel, 2003] could also contribute to the variability in Figure 7 but are not considered here. The daily variation of SHIMMER PMC occurrence frequency in Figure 7 is generally consistent with that modeled, although the calculated peaks are offset from the data by 2-3 days. The offset may be due to the fact that PMC are known to be out of phase with temperature oscillations driven by planetary waves [von Savigny *et al*., 2007; Merkel *et al*., 2008]. This phase shift cannot be simulated with our PMC parameterization, which implicitly describes all PMC formation and destruction locally and instantaneously. The meridional extent of the data in Figure 7 is between 50-58° N and with an offset of ±2-3 days, the agreement between the data and the model results is therefore adequate over length scales of ~1000 km and time scales of ~1 week.

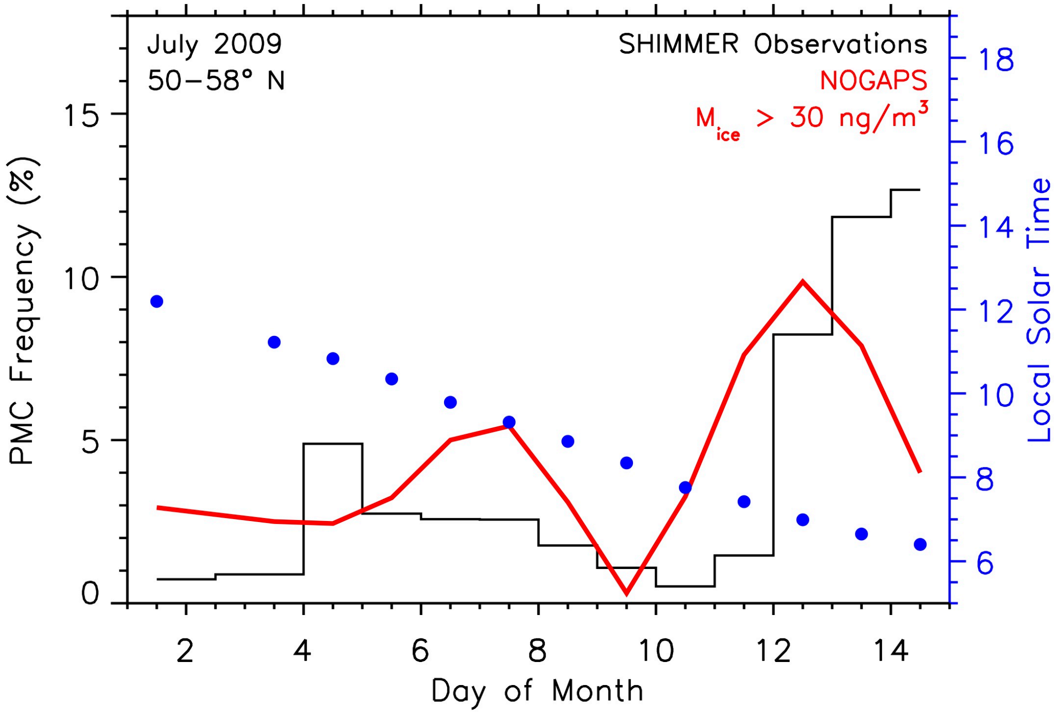

Figure 7. Daily SHIMMER PMC frequencies (black) and calculated PMC frequencies (red) between 50-58° N in in July 2009. SHIMMER observations precessed from 12 LT at the beginning of the sequence shown to 6 LT at the end of the sequence [Russell *et al.*, 2014]. The daily averaged LT is shown in blue and referenced to the right hand axis. SHIMMER observations were limited in the second half of July 2009 and are not shown. July 2 is omitted due to limited coverage that day.

We can also quantify the migrating components of the PMC IWC and frequency for the same time period. Using the same fitting procedure as with the temperature analysis in Figure 5 we determine the 24 h and 12 h amplitudes of the derived cloud properties in Figure 8 for IWC and Figure 9 for frequency. Figures 8a and 8b show the average IWC for all PMC (IWC>0 μg/m^2) and for the strong PMC (IWC>40 μg/m^2) from 48-81° N, Figures 8c and 8d show the derived amplitudes of the 24 h and 12 h components and Figures 8e and 8f show the LT for the peak of each of the components. The average IWC at 80° N is near 120 μg/m^2 in both cases because the PMC are strong enough to be well over the prescribed threshold, whereas at 50° N the IWC differ by nearly a factor of three. The amplitude of the 12 h component is weaker than the 24 h component at all northern latitudes in both cases. The peak of the 24 h oscillation is at 7 LT for mid-latitudes.

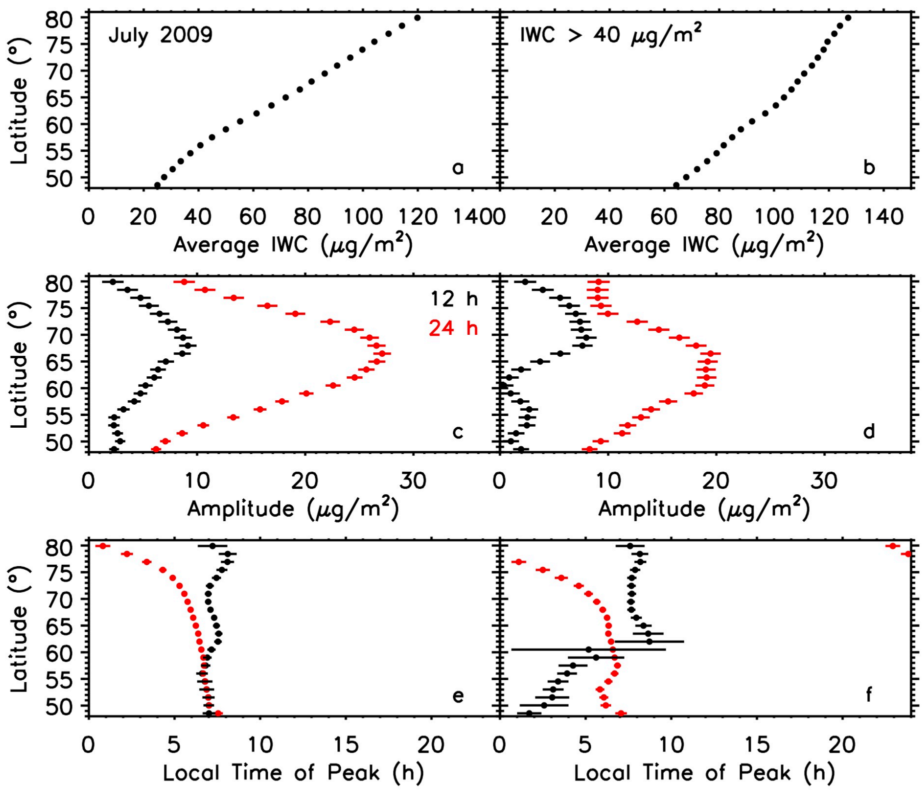

Figure 8. (a) Daily averaged IWC between 48-81° N in July 2009 for all PMC. The IWC shown is not weighted by frequency. (b) Same as Figure 8a except only strong PMC (IWC>40 $\mu g/m^2$). (c) Amplitude of the migrating 12 h and 24 h oscillation in IWC for all PMC. (d) Same as Figure 8c except for strong PMC. (e) LT for the peak of the migrating 12 h and 24 h oscillation in IWC for all PMC. (f) Same as Figure 8e except for strong PMC.

Figures 9a-9f show the results for PMC frequency using the same approach as used for IWC in Figures 8a-8f. As expected, average frequencies are near 100% in both cases near 80° N, but are only 5-20% at 50° N depending on the IWC threshold. Again, the 24 h migrating tide dominates over the 12 h tide at all latitudes shown. Note that for the 24 h tide at mid-latitudes, the amplitude of the frequency variation is comparable to the average indicating that diurnal oscillations are important in controlling the appearance of PMC at mid-latitudes. In both the case for all PMC and for strong PMC, the 24 h oscillation peaks between 5-6 LT at all latitudes shown.

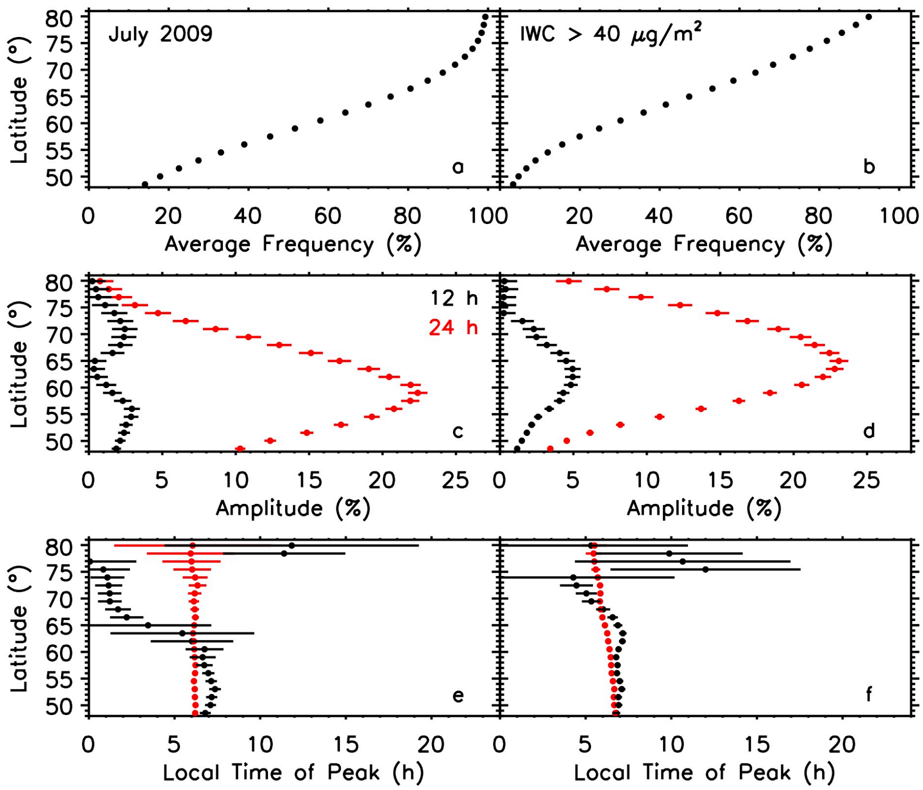

Figure 9. (a) Daily averaged PMC frequency between 48-81° N in July 2009 for all PMC. (b) Same as Figure 9a except only strong PMC. (c) Amplitude of the migrating 12 h and 24 h oscillation in frequency for all PMC. (d) Same as Figure 9c except for strong PMC. (e) LT of peak for migrating 12 h and 24 h oscillation in frequency for all PMC. (f) Same as Figure 9e except for strong PMC.

Figures 8 and 9 show that the relative variation of IWC and frequency can change significantly depending on latitude. Figures 8b and 8d show an average IWC of 118 μg/m^2 at 74° N with a 24 h amplitude of 10 μg/m^2 for strong PMC. This is a ±8% variation and in agreement with the ±7% IWC variation of DeLand and Thomas [2015] for the same latitude region. The IWC peak is at 3.6 LT at 74° N, also close to the peak of DeLand and Thomas of 2.0 LT at the same latitude. The relative 24 h variation peak in IWC for strong PMC is ±21% at 60° N. In contrast, Figures 9b and 9d show that the 24 h variation in frequency for strong PMC increases steadily from ±5% at 80° N to ±98% at 50° N. Thus, the frequency variation over the diurnal cycle is much higher than the IWC variation at mid-latitudes. Therefore, caution should be exercised when comparing different published analyses of the PMC diurnal cycle. One would expect differences between an approach which defines IWC as including the frequency dependence with analyses that define IWC solely based upon the existing clouds, independent of their frequency. Stevens *et al*. [2010] use the former approach; Deland and Thomas [2015, and references therein] use the latter approach. Figure 8 uses the Deland and Thomas definition of IWC, and the results in Figure 9 illustrate that we should expect the approaches that include frequency to become much more glaring as one moves equatorward to regions where the frequency becomes low.

3b. Southern Hemisphere: January 2008

Analogous to the approach used for the northern hemisphere, we put the NOGAPS-ALPHA one hourly temperatures on a geometric altitude grid and compare temperatures in January 2008 to SOFIE observations at 68° S. These results are shown in Figure 10a along with the SOFIE results from northern hemisphere in July 2009 for comparison, illustrating the slightly higher temperatures from January 2008. We then adjust NOGAPS-ALPHA temperature profiles at all latitudes and longitudes using the difference shown in Figure 10b. The NOGAPS-ALPHA temperatures are 2 K lower than SOFIE temperatures at 85 km and 9 K lower at 90 km. We show the adjusted NOGAPS-ALPHA temperatures for January 2008 at 85 km geometric altitude in Figures 11a (68° S) and 10b (55° S) as Hovmöller plots. The 85 km altitude is diagnostic of southern hemisphere PMC [Hervig *et al*., 2013] and slightly higher than used in the northern hemisphere (83 km). Westward traveling planetary waves are evident at mid-latitudes in Figure 11b, particularly between 2-24 January.

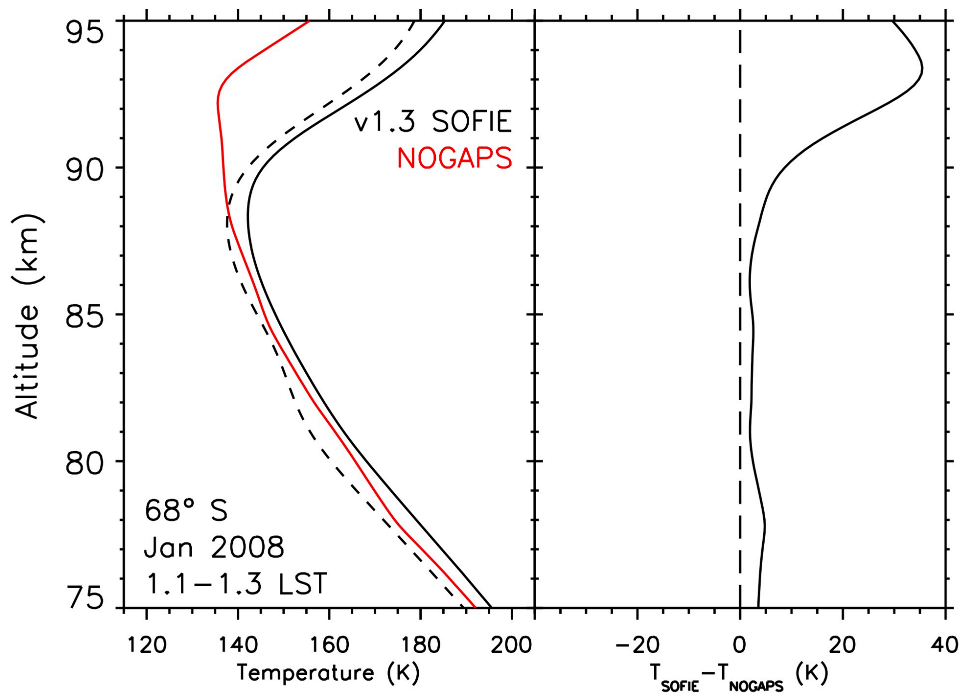

Figure 10. (a) SOFIE averaged temperatures for January 2008 (black) compared against NOGAPS-ALPHA hourly temperatures for the same latitude and LT of the SOFIE observations (red), as indicated. The SOFIE results from July 2009 (Figure 1a) are overplotted as the black dashed line for comparison. (b) The difference between the two southern hemisphere profiles in Figure 10a.

Using the temperatures in Figure 11 and interpolated water vapor from the NOGAPS-ALPHA six hourly output, we derive IWC for the same latitudes and show the results in Figure 12a (68° S) and 12b (55° S). Evidence for planetary wave activity in temperature minima of Figures 11a and 11b is reflected in the IWC in Figures 12a and 12b. As in the northern hemisphere (Figure 3), the overplotted SHIMMER PMC detections from the same time period in Figure 12b are in qualitative agreement with the calculated IWC. The location of SHIMMER PMC relative to the calculated IWC appears to be more inconsistent than in the northern hemisphere (Figure 3b). This may be due to the fact that our assumption that PMC are produced locally is less accurate when PMC variations are more affected by planetary wave activity, such as at mid-latitudes in the southern hemisphere. We will discuss these observations in the context of the different mid-latitude periodicities further below. As with the northern hemisphere case, we average the southern hemisphere results in LT to quantify the 24 h and 12 h migrating temperature tides and show those results in Figure 13.

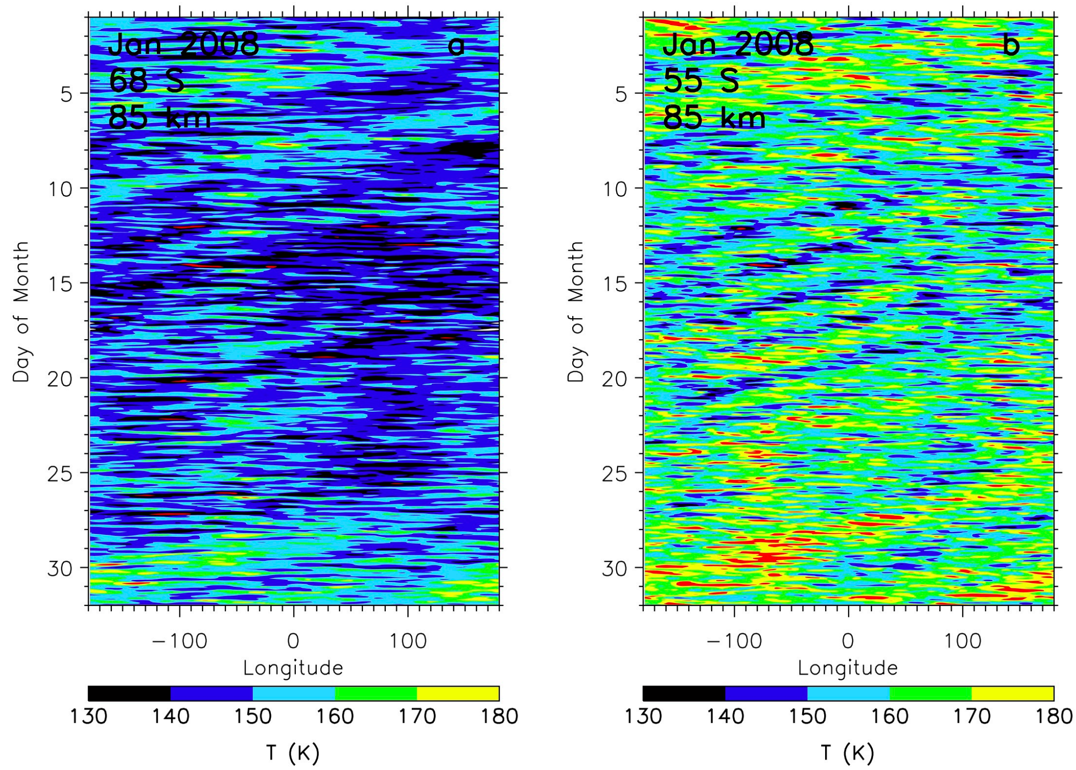

Figure 11. (a) Hovmöller plot showing temperatures for 85 km geometric altitude at 68° S during the month of January 2008. Red areas are where temperatures are in excess of 180 K. (b) Same except for 55° S.

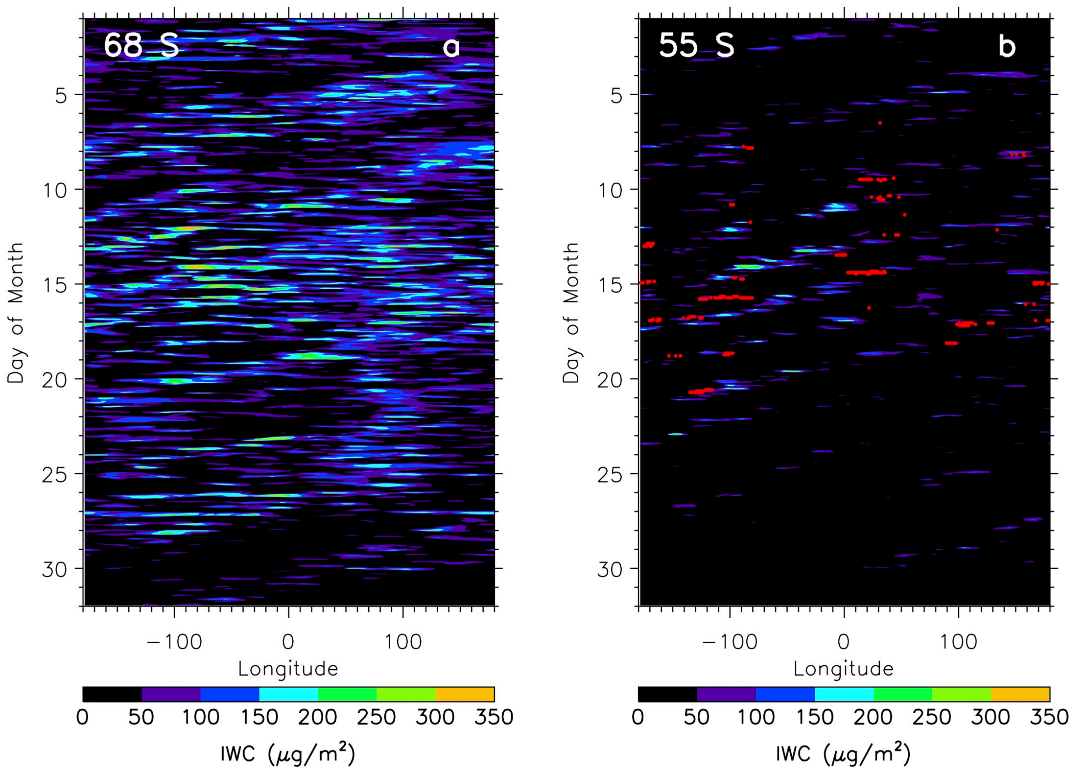

Figure 12. (a) Hovmöller plot of IWC for 68° S in January 2008. Red areas are where IWC is in excess of 300 μg/m^2. (b) Same except that IWC is shown at 55° S. Red symbols indicate where SHIMMER observed PMC from 1-31 January and between 50-58° S.

Figure 13 shows temperatures for January 2008 averaged over the diurnal cycle at four different southern latitudes where PMC are expected. On average, there is less temperature variation over the diurnal cycle in the southern hemisphere compared to the northern hemisphere, indicating that migrating tides are weaker in the south. Figure 14 shows the average temperature, amplitude and peak LT for harmonic fits to the migrating temperature tides in January 2008. The 24 h amplitudes are smaller than in the northern hemisphere and less than 2 K at all PMC latitudes. The 12 h amplitudes are larger than in the northern hemisphere but still relatively small at about 2 K or less. The peak of the 24 h oscillation is between 9-15 LT and much more variable than in the northern hemisphere.

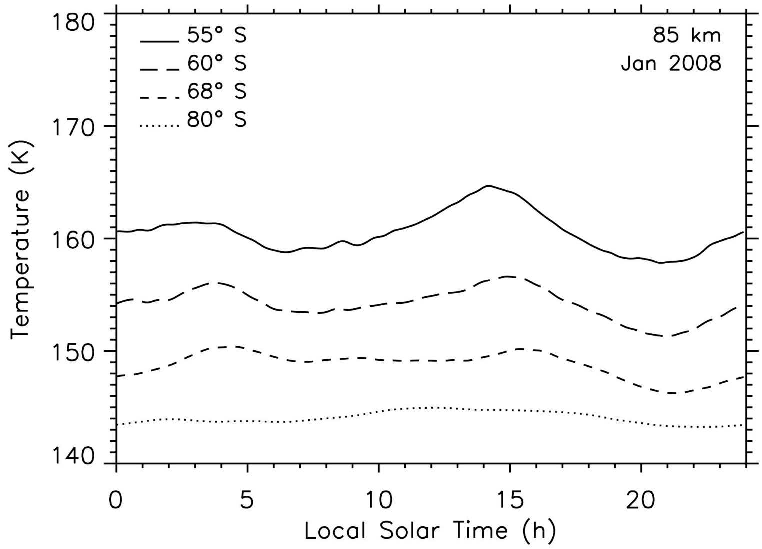

Figure 13. Average temperatures at 85 km over the diurnal cycle for January 2008 from the NOGAPS-ALPHA hourly product. The temperature over the diurnal cycle at four different PMC latitudes is shown.

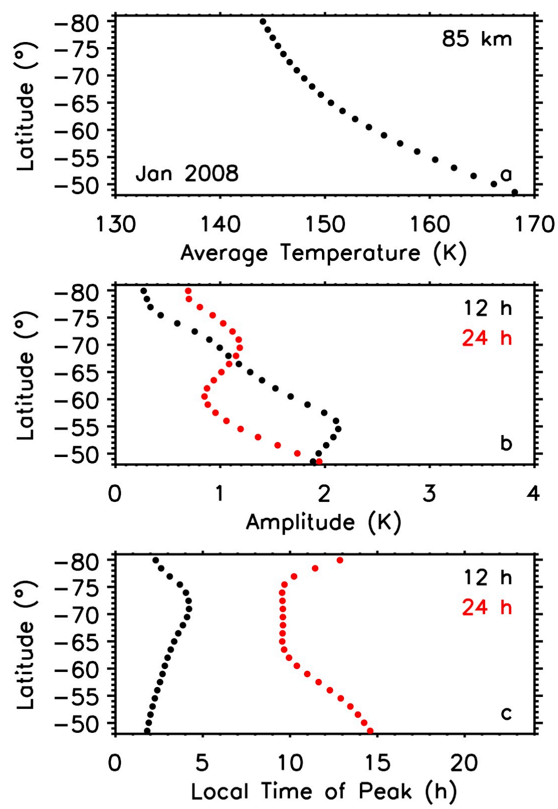

Figure 14. (a) Average temperatures at 85 km for January 2008 at 85 km from the NOGAPS-ALPHA hourly product. (b) Amplitudes of the 24 h diurnal (red) and 12 h (black) temperature tide based on harmonic fits to the temperatures. (c) LT for the peak of the 24 h (red) and 12 h (black) migrating temperature tide.

Figures 15a and 15b show calculated IWC over the diurnal cycle for four southern latitudes at which PMC form for all PMC and strong PMC, respectively. In contrast to results in the northern hemisphere, Figures 15a and 15b are distinguished by weak PMC oscillations, as expected from the temperature results in Figure 13. The IWC is 49% greater than that observed by SOFIE between 66-72º S for the same latitude and LT of the SOFIE observations. Figures 15c and 15d show PMC frequency at the same four latitudes for all PMC and strong PMC, respectively. As in the northern hemisphere, Figures 15c and 15d demonstrate the enhanced contrast over the diurnal cycle when considering only the strong PMC. The PMC frequency (70%) is slightly less than observed by SOFIE at 68° S and 1.1 LT (82%).

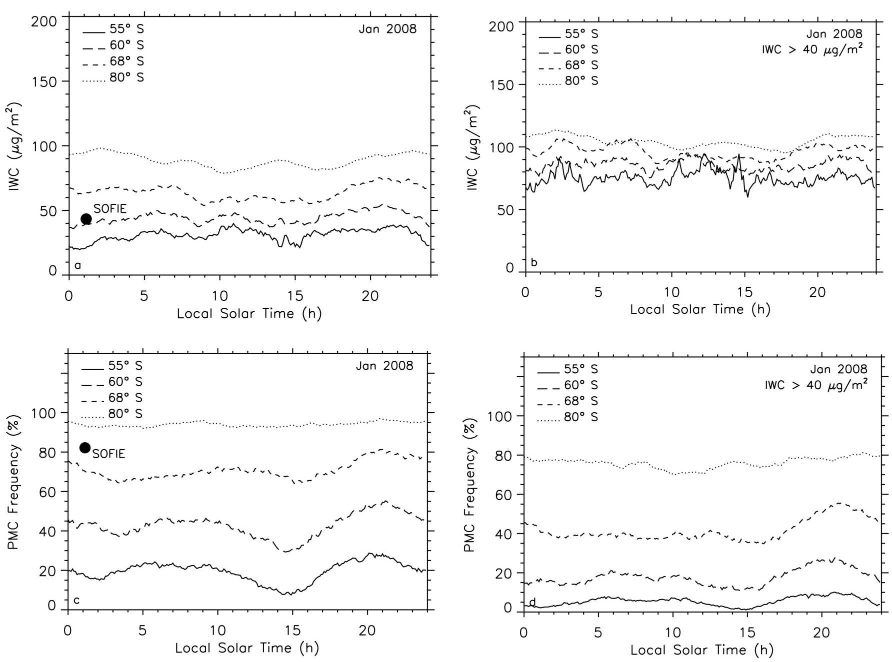

Figure 15. (a) Calculated IWC diurnal variation for January 2008 from the NOGAPS-ALPHA hourly product at four latitudes where PMC form. The IWC is not weighted by frequency and the monthly averaged SOFIE IWC (at 68° S) is indicated. (b) Same as Figure 15a but for strong PMC (IWC>40 μg/m^2). (c) Calculated PMC frequency diurnal variation at the same four latitudes. The monthly averaged SOFIE frequency is indicated. (d) Same as Figure 15c except for strong PMC.

At mid-latitudes SHIMMER was observing PMC in the southern summer throughout the daytime portion of the diurnal cycle during January 2008 and those data provide another useful means of validating our calculations. As in the northern summer case, we sample the NOGAPS-ALPHA one hourly output with the geolocated SHIMMER tangent points and simultaneously calculate PMC properties using the local temperatures, pressures and water vapor mixing ratios. The ice mass density threshold used for SHIMMER (30 ng/m^3) is the same as that used for the northern summer in Figure 7. The results are shown in Figure 16 for observations between 50-58° S, where SHIMMER observes near 14 LT on 6 January and near 8 LT on 20 January. There is a predicted peak in PMC frequency near the middle of the month as observed, with a three day phase shift similar to results in the northern hemisphere where planetary waves help to control the PMC periodicity [von Savigny *et al*., 2007; Merkel *et al*., 2008]. This frequency peak observed by SHIMMER is produced primarily by the 5 day planetary wave (see Figures 11b and 12b) since the migrating 24 h tide is weak. Other longer period planetary waves not considered here (>5 days) could also contribute to the SHIMMER peak in Figure 16. Overall for the southern summer in January 2008, the quantitative agreement with SOFIE and SHIMMER PMC observations indicate that the temperature adjustment to the analysis as well as the calculation of PMC from local conditions are an adequate way of analyzing PMC oscillations at mid-latitudes for the time period and spatial scales considered. The meridional extent of the SHIMMER data in Figure 16 is the same as for the northern hemisphere in Figure 7 so the agreement between data and model results in Figure 16 is similarly reasonable over length scales of ~1000 km and time scales of ~1 week.

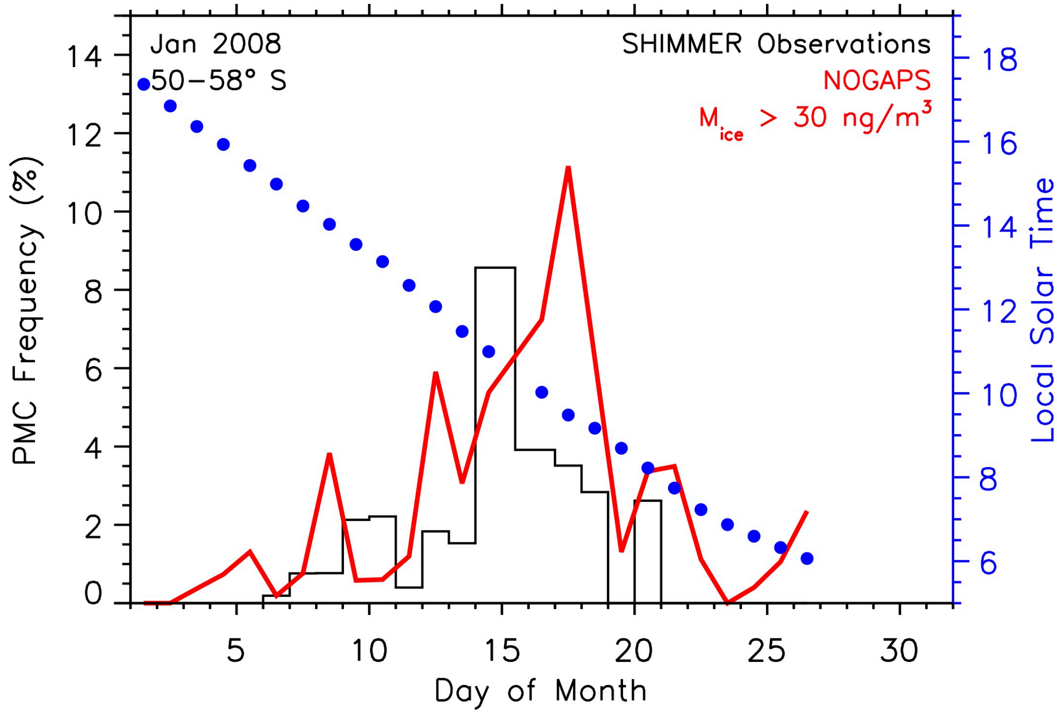

Figure 16. Daily SHIMMER PMC frequencies (black) and calculated PMC frequencies (red) between 50-58° S in in January 2008. As in Figure 7, the NOGAPS-ALPHA analysis was sampled using the geolocated SHIMMER tangent point for each orbit and the same ice mass density detection threshold was used. The daily averaged local solar time is shown in blue and referenced to the right hand axis.

Figures 17a-17f show the average IWC, derived amplitude and LT for the peaks of all PMC and strong PMC in January 2008, analogous to the northern summer analysis in Figure 8. Peak amplitudes of 24 h and 12 h migrating oscillations (<8 μg/m^2) are over a factor of two less than peak amplitudes in the northern summer. These IWC oscillations in the southern summer are more variable due to the weaker amplitudes. Figures 18a-18f show the average PMC frequency, amplitude and LT for the peaks of all PMC and strong PMC over the same time period. The figures are distinguished primarily by their peak amplitudes, which are a factor of four to five less than the northern summer (Figure 9). In the next section we analyze the NOGAPS-ALPHA temperature fields for nonmigrating tides and planetary waves.

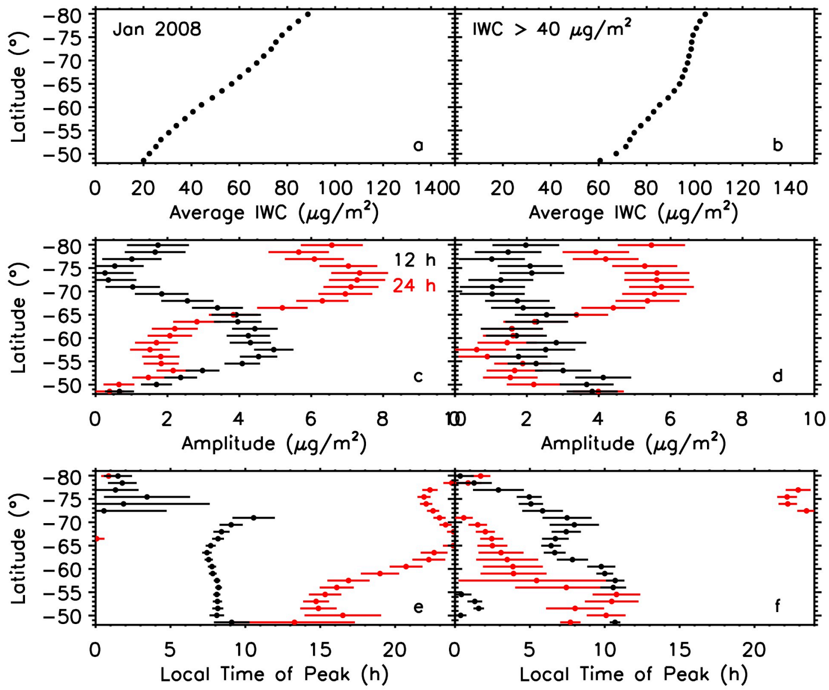

Figure 17. (a) Daily averaged IWC between 48-81° S in January 2008 for all PMC. The IWC shown is not weighted by frequency. (b) Same as Figure 17a except only bright PMC (IWC>40 $\mu g/m^2$). (c) Amplitude of the migrating 24 h and 12 h oscillations in IWC for all PMC. (d) Same as 17c except for bright PMC. (e) LT for peak of migrating 24 h and 12 h oscillation in IWC for all PMC. (f) Same as Figure 17e except for strong PMC.

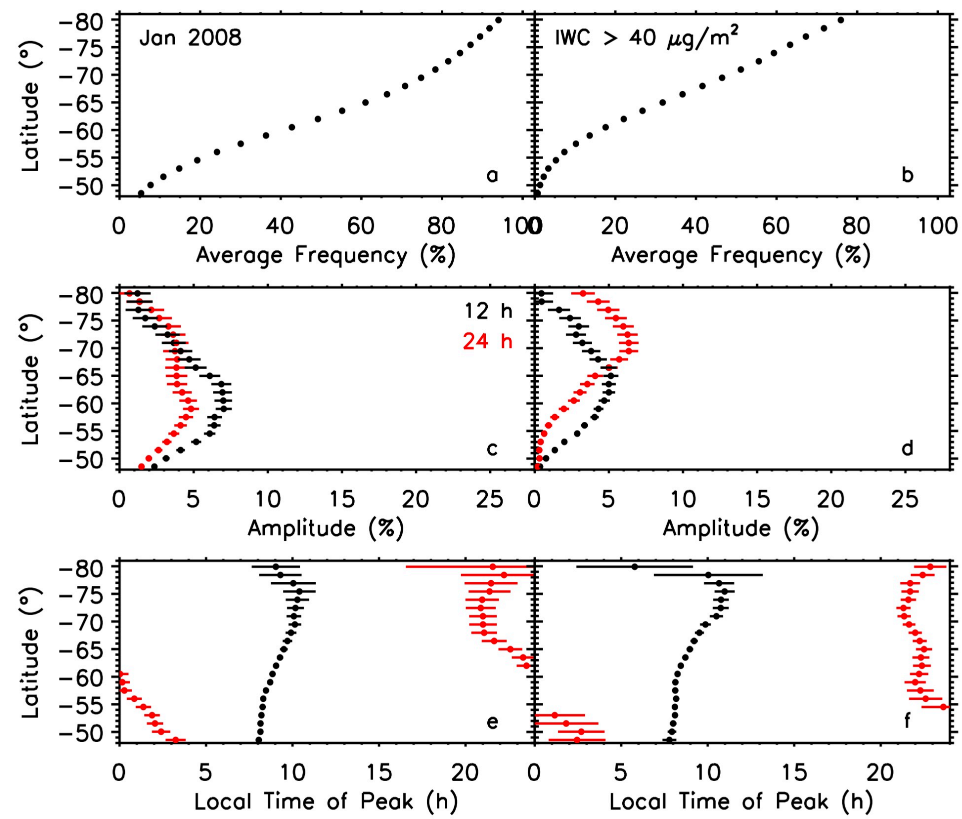

Figure 18. (a) Daily averaged PMC frequency between 48-81° N in July 2009 for all PMC. (b) Same as Figure 18a except only bright PMC (IWC>40 μg/m^2). (c) Amplitude of the migrating 24 h and 12 h oscillation in frequency for all PMC. (d) Same as 18c except for bright PMC. (e) LT for peak of migrating 24 h and 12 h oscillation in frequency for all PMC. (f) Same as Figure 18e except for strong PMC.

4. Nonmigrating Tides and Planetary Waves

In Section 3 we demonstrated how migrating temperature tides derived from the NOGAPS-ALPHA hourly output are directly related to PMC oscillations. We moreover showed that the derived PMC properties were consistent with existing PMC observations for the same time periods analyzed. However, by binning the output in LT for the month we averaged out contributions from nonmigrating tides and planetary waves. In this section we use different approaches to provide a quantitative analysis of nonmigrating tides and planetary waves.

4a. Nonmigrating Tides

Analysis of nonmigrating temperature tides begins with re-binning the NOGAPS-

ALPHA hourly product from the native 2° × 2° latitude-longitude grid to a coarser 5° × 24° latitude-longitude grid. This re-binning facilitates the computations, which are done on a global scale and at all altitudes. The maximum resolvable wavenumber of any component on this grid is seven, which sufficiently captures the wavenumbers accounting for much of the tidal variability in the mesosphere and lower thermosphere [Zhang *et al*., 2006; Oberheide *et al*., 2006; 2007]. Daily data at this coarser spatial resolution are then interpolated to geometric altitude levels, and sorted into one hourly universal time bins. For investigations of monthly mean tidal behavior, we average monthly data within each hourly bin to obtain composite 24-hour sequences at each latitude, longitude and altitude.

Diurnal, semidiurnal and terdiurnal (8 h) harmonics are computed via Fourier analysis of the composite 24-hour time series at each grid point. These harmonics are defined as

$$T_n(t) = A_n\cos(n\omega t) + B_n\sin(n\omega t)$$

with n = 1 (2) for the diurnal (semidiurnal) harmonic. Migrating tides are computed as the nth zonal wave component of the nth fraction of the 24-hour period. Thus, the migrating diurnal (semidiurnal) tide is the zonal wavenumber 1 (2) component of the 24 (12) hour harmonic. Mathematically, a migrating tide is expressed for each longitude λ as

$$T_{n\_mig}(t, \lambda) = A_{n\_mig}\cos[n(\lambda+\omega t)] + B_{n\_mig}\sin[n(\lambda+\omega t)]$$

Nonmigrating tides at each longitude are computed as the vector difference between $T_n(t)$ and the corresponding migrating tide. The nonmigrating diurnal tide is therefore evaluated at each longitude λ as

$$T_{1\_nonmig}(t, \lambda) = A_1\cos(\omega t) - A_{1\_mig}\cos(\lambda+\omega t) + B_1\sin(\omega t) - B_{1\_mig}\sin(\lambda+\omega t)$$

The separation of nonmigrating from migrating tidal components represents a significant advance to middle atmosphere tidal analyses of temperature and PMC as observations from a single ground-based station are not suitable for this [*e.g.* Lübken *et al*., 2011; Kopp *et al*., 2015] and satellite observations alone do not have the temporal resolution to resolve these components synoptically.

Figure 19 shows a sample of results for derived tidal harmonics at 55° N and 12 UT for all longitudes. This latitude and time period is chosen to represent a day and latitude of relatively high PMC frequency observed by SHIMMER (Figure 7). The solution to the fit of the data is shown in the top panel and the migrating and nonmigrating tidal components are split out in the middle and bottom panels, respectively. The 24 h migrating tide dominates in the middle panel whereas the nonmigrating components are more variable than the migrating components but together contribute significantly to the NOGAPS-ALPHA temperature variation in the top panel.

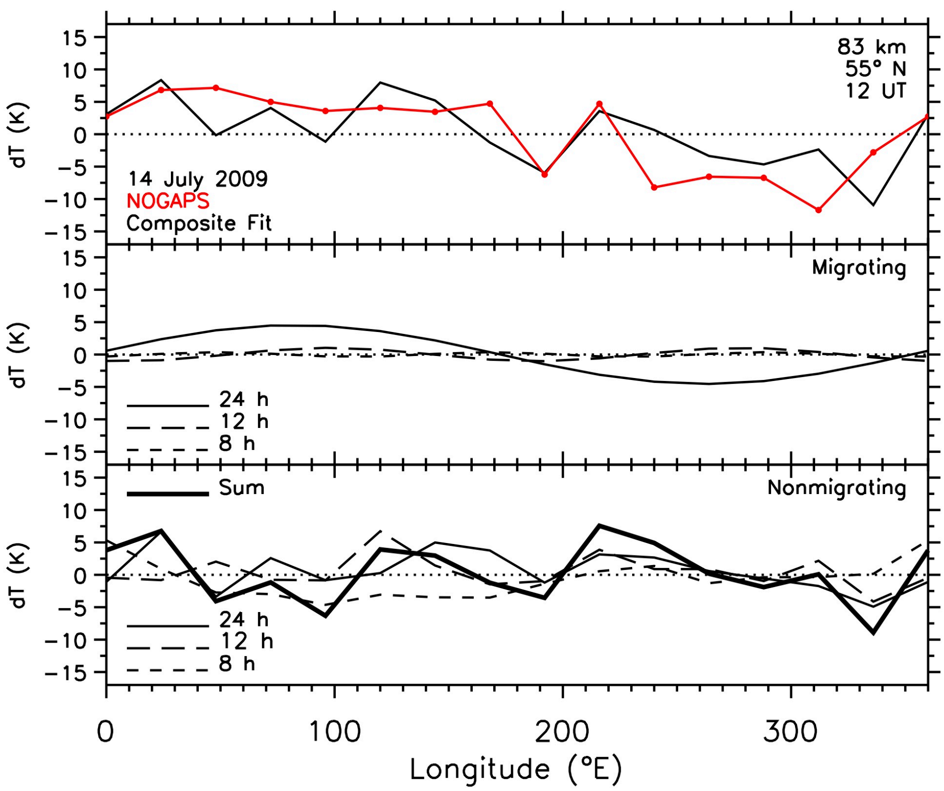

Figure 19. (top) NOGAPS-ALPHA temperature variation at 55° N and 12 UT for all longitudes. The NOGAPS-ALPHA binned data used in the nonmigrating analysis is shown in solid red. Also shown is the best fit solution calculated as Fourier harmonics (black, see text). (middle) the migrating tides for the 24 h component (solid black), 12 h component (long dashed) and 8 h

component (short dashed). (bottom) Same as middle panel except for the nonmigrating components. The sum of all of the nonmigrating components is also included as a thick line.

4b. Planetary Waves

Using the six hourly NOGAPS-ALPHA analysis, McCormack *et al*. [2014] studied the interannual variability of the 2 day planetary wave in the summertime between 2007-2009. Using a fast Fourier transform approach to the temperature fields, they found the 2 day wave in temperature peaks during the summer in the upper mesosphere with an amplitude of 2-3 K. Vertical wavelengths for planetary waves are about 100 km [Lilienthal and Jacobi, 2015] and we focus here on deriving planetary wave temperature amplitudes at a pressure level of 0.006 hPa, which corresponds to a geometric altitude of approximately 85 km to be consistent with the altitudes of our analyses throughout this work.

The two-dimensional fast Fourier transform (2DFFT) described in McCormack *et al*. [2009] expands NOGAPS-ALPHA temperature fields at a given latitude and pressure level as Fourier series in longitude and time. Zonal means are first subtracted from each six-hourly longitude-time field and then a cosine taper is applied to the first and last 10% of each record in time. The 2DFFT is applied over a 32-day interval (128 points) to derive results for an individual month, and the resulting space-time power spectra describe the amount of variance at each frequency and zonal wave number.

To isolate the behavior of the 2 day and 5 day wave in the NOGAPS-ALPHA temperature analyses, six hourly longitude/time fields are reconstructed by applying band-pass filters to the inverse 2DFFT. Inspection of the 2DFFT power spectra for both northern and southern summer periods indicate that the variance associated with the zonal wave number 3 2 day wave lies within the 0.40 -- 0.56 cycles per day (cpd) range, while the variance associated with the zonal wave number one 5 day wave lies within the pass bands from 0.16 -- 0.25 cpd. Using these bands, the root mean square amplitudes of the zonal wave number 1 and 3 components are then calculated from the filtered fields at each latitude and pressure every six hours, from which monthly means are then computed. This technique has been applied previously to NOGAPS-ALPHA fields to investigate characteristics of the 2 day wave and migrating diurnal tide in the mesosphere [see, *e.g*., McCormack *et al*., 2010; McCormack *et al*. 2014]. In the present study, we extend this analysis to focus on the 2 day and 5 day wave during northern and southern summers. Monthly averaged 2 day and 5 day wave amplitudes along with all other amplitudes derived in this study as a function of latitude are overplotted in Figure 20 (northern hemisphere) for July 2009 and in Figures 21a-21c (southern hemisphere) for January 2008-2010.

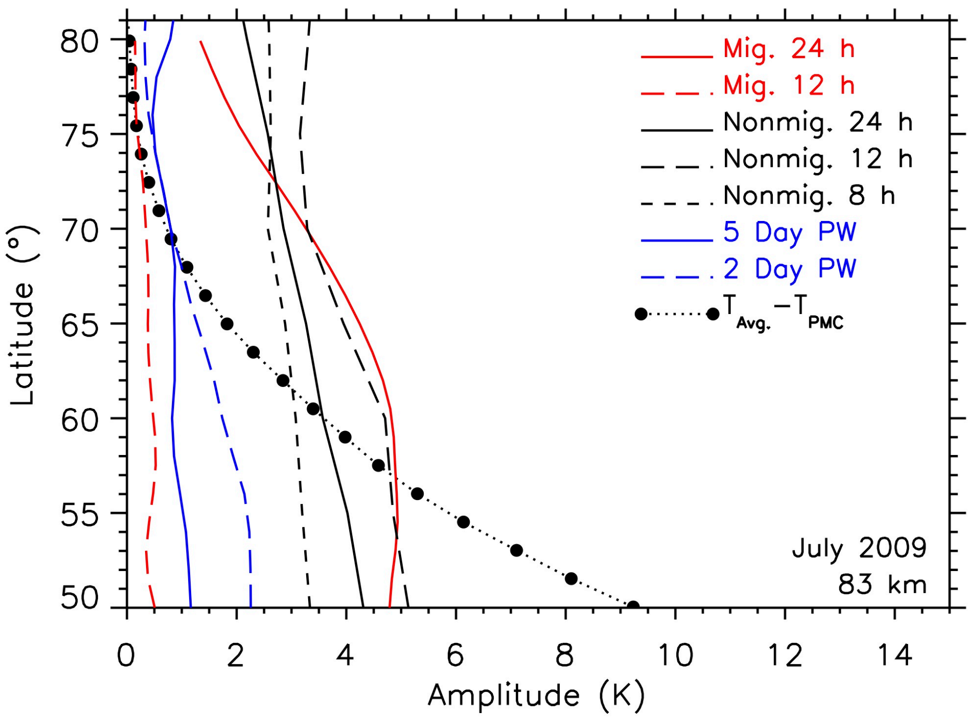

Figure 20. Monthly averaged amplitudes of all migrating (red), nonmigrating (black) and planetary wave (blue) components in July 2009 for northern latitudes at 83 km, where PMC are

observed. Also included is the zonally averaged temperature difference between the ambient temperature and the temperature where there are PMC ($T_{Avg.}$-T_{PMC}, dotted line with symbols). Although the migrating diurnal tide is strong, the amplitudes of the nonmigrating tides are collectively the most important source of PMC, particularly at mid-latitudes.

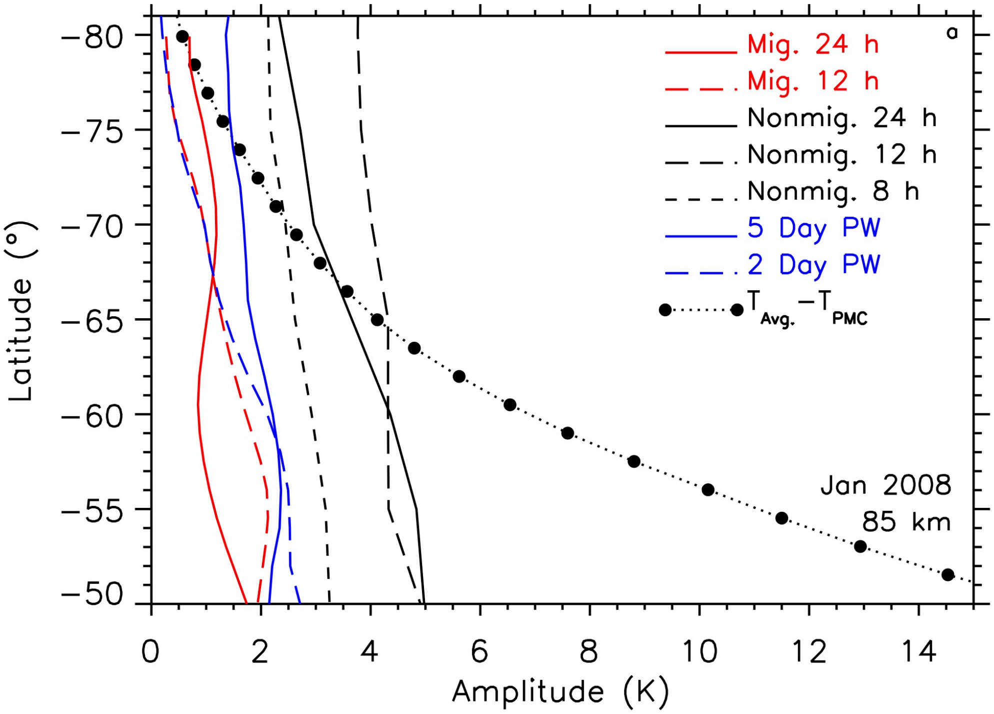

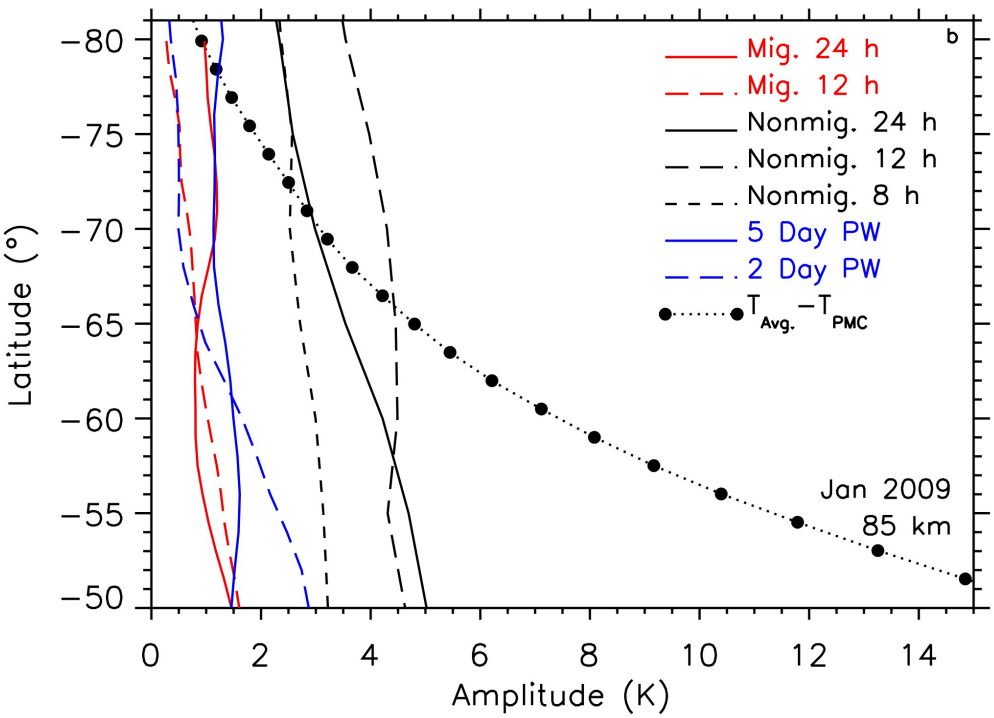

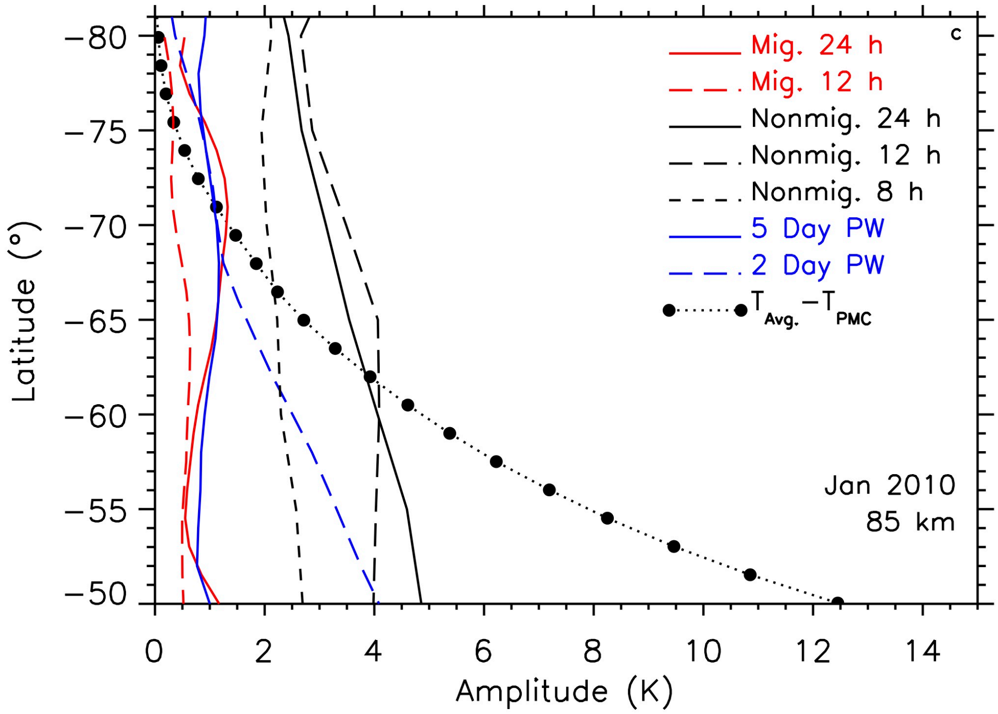

Figure 21. (a) Same as Figure 20 except for the southern high latitudes in January 2008 at 85 km, where PMC are observed in the southern hemisphere. The nonmigrating tides dominate PMC formation. (b) Same as panel (a) except the results are for January 2009. (c) Same as panel (a) except for January 2010.

5. Discussion

Figure 20 shows that between 50-75° N the most important processes driving PMC periodicities in the northern hemisphere are the 24 h migrating and 12 h nonmigrating tides, with amplitudes for both between 2-5 K. Throughout the northern PMC region all three nonmigrating components (24 h, 12 h and 8 h) contribute substantially with average amplitudes for each of them between 2-5 K. Note that the amplitudes of the nonmigrating components tend to increase at mid-latitudes. The amplitudes for these tidal components are all larger than those for the 2 day and 5 day planetary waves in the northern hemisphere. Longer period planetary waves such as the 16 day wave can have significant amplitudes of up to 5 K in the summer polar mesosphere [*e.g.* Espy and Witt, 1996; Espy *et al*., 1997]. However, in July 2009 the amplitude was small (<2 K), which is typical of the period from 2005-2010 in the polar summer [Day *et al*., 2011; McDonald *et al*., 2011]. Also shown in Figure 20 is the difference between the average temperature at each latitude and the temperature where there is a PMC present at the same latitude. This difference represents the downward temperature excursion needed to create a PMC, which increases significantly at lower latitudes.

We similarly show averaged amplitudes as a function of southern latitudes in Figures 21a, 21b and 21c for January 2008, January 2009 and January 2010, respectively. Figures 21a-21c show that in contrast to the northern hemisphere, the 24 h migrating tide only plays a minor role in contributing to the temperature periodicities. The nonmigrating tides dominate for all three time periods, with amplitudes for each between 2-5 K, also increasing to lower latitudes.

Planetary waves also can combine to contribute significantly to PMC formation. The monthly averaged 2 day and 5 day planetary wave amplitudes in Figures 20 and 21 are generally between 1-4 K from 50-70° latitude. These results are consistent with previous work [von Savigny *et al*., 2007; Merkel *et al*., 2008; Dalin *et al*., 2011] showing that maximum amplitudes for these waves were between 2.0-3.5 K in the polar summer mesosphere. Planetary wave amplitudes can be larger (4-6 K) depending on the part of the month sampled as indicated in Figures 2 and 11.

It is important to note that the average nonmigrating tidal amplitudes in Figures 20 and 21 are also highly variable on hourly time scales. Standard deviations of the 12 h and 24 h variability calculated from both the hourly and longitudinal geophysical variation are 1-3 K at all PMC latitudes in both hemispheres. This variability of the nonmigrating tides and planetary wave amplitudes is in contrast to the more stable 24 h migrating tide for which the standard deviation is 1 K or less in both hemispheres.

Previous mid-latitude ground-based observations reported by Gerding *et al*. [2013b] from Kühlungsborn, Germany (54° N) indicated a temperature minimum around noon in the mesopause region. Gerding *et al*. also observed an early morning peak in mesospheric clouds, which helped lead to the suggestion by Gerding *et al*. that meridional transport from higher latitudes is the main driver for mid-latitude mesospheric cloud occurrence between 2010-2013. In contrast to their results, our results using global-scale assimilated satellite data from July 2009 indicate a mid-latitude temperature minimum near 6 LT that is more consistent with the early morning peak in mesospheric clouds.

6. **Summary**

Our global assimilation/forecast system enables the quantification of the largest mesospheric temperature oscillations including migrating and nonmigrating temperature tides as well as the 2 day and 5 day planetary waves. Producing output at an hourly cadence furthermore allows for quantitative study of the 12 h migrating tidal component as well as the 12 h and 8 h nonmigrating tidal components, which is not possible using a cadence of six hours as in previous studies. We focus primarily on July 2009 (northern summer) and January 2008 (southern summer) to derive oscillations at latitudes and altitudes relevant to PMC formation. We have quantified periodicities due to the most important migrating and nonmigrating temperature components as well as their consequent impact on PMC periodicities.

We find that the 24 h migrating tide together with the 24 h and 12 h nonmigrating tides dominate monthly averaged PMC oscillations in the northern summer with amplitudes between 2-5 K for each of these components throughout most of the PMC region (50-75° N). The larger amplitudes in this range are generally found at lower PMC latitudes. The calculated IWC variation over the diurnal cycle for the 24 h migrating tide is consistent with SBUV observations reported by DeLand and Thomas [2015]. The monthly averaged amplitudes for the 2 day and 5 day planetary waves are 1-3 K but can sporadically be as high as 4-6 K.

In the southern summer the migrating components are much weaker and the nonmigrating components dominate the monthly averaged oscillations. For January 2008, the monthly averaged 12 h and 24 h nonmigrating amplitudes vary from 2-5 K throughout the PMC region, generally increasing from higher to lower PMC latitudes. Nonmigrating temperature tides have similar amplitudes and also dominate over migrating tides for January 2009 and January 2010. The 2 day and 5 day planetary waves contribute to monthly averaged temperature oscillations in the southern summer, with monthly averaged amplitudes between 1-4 K from 50-70° S. The various components identified and their superposition help to identify what determines PMC formation at any given time, particularly at mid-latitudes.

Over horizontal length scales of 1000 km and time scales of a week, a description of PMC frequency and IWC can be approximated by only the local temperature, pressure and water vapor concentrations at both high and mid latitudes. PMC oscillations due to planetary waves with periods less than a week may require a more complex microphysical model than we use as these oscillations are known to be out of phase with temperature oscillations [von Savigny *et al*., 2007; Merkel *et al*., 2008]. Our calculated PMC properties are in agreement with concurrent IWC satellite observations of SOFIE near 68° N and 68° S as well as concurrent PMC observations by SHIMMER from 50-58° N and 50-58° S.

The use of a high-altitude data assimilation/forecast system yields a more complete analysis of intra-seasonal PMC oscillations than is possible using mesospheric satellite data alone. The global-scale nature of our analysis will inform intra-seasonal studies of other temperature and PMC datasets and help to guide future work on longer term temperature and PMC variations.

Acknowledgements. This work was supported by the NASA Heliophysics Supporting Research program and the NASA AIM mission. The NOGAPS-ALPHA analysis at hourly cadence can be found via anonymous ftp at map.nrl.navy.mil in /pub/nrl/nogaps. The AIM/SOFIE data can be downloaded from sofie.gats-inc.com. The SHIMMER data may be downloaded from the NASA SPDF archive site at ftp://spdf.gsfc.nasa.gov/pub/data/shimmer/. SHIMMER is a joint program between the Naval Research Laboratory and the DoD Space Test Program.

References

Baumgarten, G. *et al*., On the horizontal and temporal structure of noctilucent clouds as observed by satellite and lidar at ALOMAR (69N), *Geophys. Res. Lett*., **39**, L01803, doi:10.1029/2011GL049935, 2012.

Dalin, P. *et al*., A case study of the evolution of a Kelvin-Helmholtz wave and turbulence in noctilucent clouds, *J. Atm. Sol.-Terr. Phys*., **72**, 1129-1138, 2010.

Dalin, P. *et al*., A comparison between ground-based observations of noctilucent clouds and Aura satellite data, *J. Atm. Sol.-Terr. Phys*., **73**, 2097-2109, 2011.

Day, K.A., R.E. Hibbins, and N.J. Mitchell, Aura MLS observations of the westward-propagating s=1, 16-day planetary wave in the stratosphere, mesosphere and lower thermosphere, *Atmos. Chem. Phys*., **11**, 4149-4161, 2011.

DeLand, M.T. and G.E. Thomas, Updated PMC trends derived from SBUV data, *J. Geophys. Res*., **120**, 2140-2166, doi:10.1002/2014JD022253, 2015.

DeLand, M.T., E.P. Shettle, G.E. Thomas, and J.J. Olivero, Direct observations of PMC local time variations by Aura OMI, *J. Atm. Sol.-Terr. Phys*., **73**, 2049-2064, 2011.

Eckermann, S.D. *et al*., High-altitude data assimilation system experiments for the northern summer mesosphere season of 2007, *J. Atm. Sol.-Terr. Phys*., **71**, 531-551, 2009.

Englert, C.R., M.H. Stevens, D.E. Siskind, J.M. Harlander, and F.L. Roesler, Spatial Heterodyne Imager for Mesospheric Radicals on STPSat-1, *J. Geophys. Res*., **115**, D20306, doi:10.1029/2010JD014398, 2010.

Espy, P.J. and G. Witt, Observation of a quasi 16-day oscillation in the polar summer mesospheric temperature, *Geophys. Res. Lett*., **23**, 1071-1074, 1996.

Espy, P.J., J. Stegman and G. Witt, Interannual variations of the quasi-16-day oscillation in the polar summer mesospheric temperature, *J. Geophys. Res.*, **102**, 1983-1990, 1997.

Fiedler, J., G. Baumgarten, and G. von Cossart, Mean diurnal variations of noctilucent clouds during 7 years of lidar observations at ALOMAR, *Annales Geophysicae*, **23**, 1175-1181, 2005.

Fiedler, J. *et al*., NLC and the background atmosphere above ALOMAR, *Atmos. Chem. Phys*., **11**, 5701-5717, 2011.

Gerding, M. *et al*., Simultaneous observation of noctilucent clouds, mesospheric summer echoes, and temperature at a midlatitude station (54° N), *J. Geophys. Res*., **112**, D12111, doi:10.1029/2006JD008135, 2007.

Gerding, M., J. Hoffner, P. Hoffmann, M. Kopp, and F.-J. Lubken, Noctilucent cloud variability and mean parameters from 15 years of lidar observations at a mid-latitude site (54º N, 12º E), *J. Geophys. Res*., **118**, 317-328, doi:10.1029/2012JD018319, 2013a.

Gerding, M., M. Kopp, P. Hoffmann, J. Hoffner, and F.-J. Lubken, Diurnal variations of midlatitude NLC parameters observed by daylight-capable lidar and their relation to ambient paramters, *Geophys. Res. Lett*., **40**, 6390-6394, doi: 10.1002/2013GL057955, 2013b.

Gumbel, J. and B. Karlsson, Intra- and inter-hemispheric coupling effects on the polar summer mesosphere, *Geophys. Res. Lett*., **38**, L14804, doi:10.1029/2011GL047968, 2011.

Herron, J.P., V.B. Wickwar, P.J. Espy, and J.W. Meriwether, Observations of a noctilucent cloud above Logan, Utah (41.7°N, 111.8°W) in 1995, *J. Geophys. Res*., **112**, D19203, doi:10.1029/2006JD007158, 2007.

Hervig, M. and D.E. Siskind, Decadal and inter-hemispheric variability in polar mesospheric clouds, water vapor, and temperature, *J. Atm. Sol.-Terr. Phys*., **68**, 30-41, 2006.

Hervig, M.E. and M.H. Stevens, Interpreting the 35 year SBUV PMC record with SOFIE observations, *J. Geophys. Res.*, **119**, doi:10.1002/2014JD021923, 2014.

Hervig, M.E. *et al.*, Relationships between polar mesospheric clouds, temperature, and water vapor from Solar Occultation for Ice Experiment (SOFIE) observations, *J. Geophys. Res.*, **114**, D20203, doi:10.1029/2009JD012302, 2009.

Hervig, M.E., D.E. Siskind, M.H. Stevens, L.E. Deaver, Inter-hemispheric comparison of PMCs and their environment from SOFIE observations, *J. Atm. Sol.-Terr. Phys.*, **104**, 285-298, 2013.

Hervig, M.E., D.E. Siskind, S.M. Bailey, J.M. Russell III, The influence of PMCs on water vapor and drivers behind PMC variability from SOFIE observations, *J. Atm. Sol.-Terr. Phys.*, **132**, 124-134, 2015.

Hervig, M.E., U. Berger and D.E. Siskind, Decadal variability in PMCs and implications for changing temperature and water vapor in the upper mesosphere, *J. Geophys. Res.*, **121**, doi:10.1002/2015JD024439, 2016a.

Hervig, M.E. *et al.*, Mid-latitude mesospheric clouds and their environment from SOFIE observations, *J. Atm. Sol.-Terr. Phys.*, **149**, 1-14, 2016b.

Hoppel, K.W. *et al.*, Assimilation of stratospheric and mesospheric temperatures from MLS and SABER in a global NWP model, *Atmos. Chem. Phys.*, **8**, 6103-6116, 2008.

Hultgren, K. *et al.*, What caused the exceptional mid-latitudinal Noctilucent Cloud event in July 2009, *J. Atm. Sol.-Terr. Phys.*, **73**, 2125-2131, 2011.

Karlsson, B. *et al.*, Intra-seasonal variability of polar mesospheric clouds due to inter-hemispheric coupling, *Geophys. Res. Lett.*, **36**, L20802, doi:10.1029/2009GL040348, 2009.

Kirkwood, S. and K. Stebel, Influence of planetary waves on noctilucent cloud occurrence over NW Europe, *J. Geophys. Res*., **108**, 8440, doi:10.1029/2002JD002356, 2003.

Kopp, M., M. Gerding, J. Höffner, F.-J. Lübken, Tidal signatures in temperatures derived from daylight lidar soundings above Kühlungsborn (54°N, 12°E), **127**, 37-50, 2015.

Lieberman, R.S., D.M. Riggin, D.A. Ortland, J. Oberheide, and D.E. Siskind, Global observations and modeling of nonmigrating diurnal tides generated by tide-planetary wave interactions, *J. Geophys. Res*., **120**, doi:10.1002/2015JD023739, 2015.

Lilienthal, F. and Ch. Jacobi, Meteor radar quasi 2-day wave observations over 10 years at Collm (51.3° N, 13.0° E), *Atmos. Chem. Phys*. **15**, 9917-9927, 2015.

Lübken, F.-J., J. Höffner, T.P. Viehl, B. Kaifler, and R.J. Morris, First measurements of thermal tides in the summer mesopause region at Antarctic latitudes, *Geophys. Res. Lett*., **38**, L24806, doi:10.1029/2011GL050045, 2011.

McCormack, J. P., L. Coy, and K. W. Hoppel, Evolution of the quasi 2-day wave during January 2006, *J. Geophys. Res*., **114**, D20115, doi:10.1029/2009JD012239, 2009.

McCormack, J. P., S. D. Eckermann, K. W. Hoppel, and R. A. Vincent, Amplification of the quasi-two day wave through nonlinear interaction with the migrating diurnal tide, *Geophys. Res. Lett*., **37**, L16810, doi:10.1029/2010GL043906, 2010.

McCormack, J.P., L. Coy, and W. Singer, Intraseasonal and interannual variability of the quasi 2 day wave in Northern Hemisphere summer mesosphere, *J. Geophys. Res*., **119**, 2928-2946, doi:10.1002/2013JD020199, 2014.

McDonald, A.J., R.R. Hibbins, and M.J. Jarvis, Properties of the quasi 16 day wave derived from EOS MLS observations, *J. Geophys. Res*., **116**, D06112, doi:10.1029/2010JD014719, 2011.

Merkel, A.W., R.R. Garcia, S.M. Bailey, and J.M. Russell III, Observational studies of planetary waves in PMCs and mesospheric temperature measured by SNOE and SABER, *J. Geophys. Res*., **113**, D14202, doi:10.1029/2007JD009396, 2008.

Nielsen, K. *et al*., On the origin of mid-latitude mesospheric clouds: The July 2009 cloud outbreak, *J. Atm. Sol.-Terr. Phys*., **73**, 2118-2124, 2011.

Oberheide, J., Q. Wu, T.L. Killeen, M.E. Hagan, and R.G. Roble, Diurnal nonmigrating tides from TIMED Doppler Interferometer wind data: Monthly climatologies and seasonal variations, *J. Geophys. Res*., **111**, A10S03, doi: 10.1029/2005JA011491, 2006.

Oberheide, J., Q. Wu, T.L. Killeen, M.E. Hagan, and R.G. Roble, A climatology of nonmigrating semidiurnal tides from TIMED Doppler Interferometer (TIDI) wind data, *J. Atm. Sol.-Terr. Phys*., **69**, 2203-2218, 2007.

Pancheva, D., P. Mukhtarov, D.E. Siskind, and A.K. Smith, Global distribution and variability of quasi 2 day waves based on the NOGAPS-ALPHA reanalysis model, *J. Geophys. Res*., **121**, doi:10.1002/2016JA023381, 2016.

Pertsev, N. *et al*., Noctilucent clouds observed from the ground: sensitivity to mesospheric parameters and long-term time series, *Earth, Planets and Space*, **66**:98, 2014.

Rapp, M. and G.E. Thomas, Modeling the microphysics of mesospheric ice particles: Assessment of current capabilities and basic sensitivities, *J. Atm. Sol.-Terr. Phys*., **68**, 715-744, 2006.

Rapp, M., F.-J. Lubken, A. Mullemann, G.E. Thomas and E.J. Jensen, Small-scale temperature variations in the vicinity of NLC: Experimental and model results, *J. Geophys. Res.*, **107**, 4392, doi:10.1029/2001JD001241, 2002.

Remsberg, E.E. *et al*., Assessment of the quality of the Version 1.07 temperature-versus-pressure profiles of the middle atmosphere from TIMED/SABER, *J. Geophys. Res*., **113**, D17101, doi:10.1029/2008JD010013, 2008.

Rong, P.P., J.M. Russell III, M.E. Hervig and S.M. Bailey, The roles of temperature and water vapor at different stages of the polar mesospheric cloud season, *J. Geophys. Res*., **117**, D04208, doi:10.1029/2011JD016464, 2012.

Rong, P.P., J.M. Russell III, C.E. Randall, S.M. Bailey, and A. Lambert, Northern PMC brightness zonal variability and its correlation with temperature and water vapor, *J. Geophys. Res*., **119**, 2390-2408, doi:10.1002/2013JD020513, 2014.

Russell, J.M. III, P. Rong, S.M. Bailey, M.E. Hervig, and S.V. Petelina, Relationship between the summer mesopause and polar mesospheric cloud heights, *J. Geophys. Res*., **115**, D16209, doi:10.1029/2010JD013852, 2010.

Russell, J.M. III *et al*., Analysis of northern midlatitude noctilucent cloud occurrences using satellite data and modeling, *J. Geophys. Res*., **119**, doi:10.1002/2013JD021017, 2014.

Schwartz, M.J. *et al*., Validation of the Aura Microwave Limb Sounder temperature and geopotential height measurements, *J. Geophys. Res*., **113**, D15811, doi:10.1029/2007JD008783, 2008.

Shettle, E.P., M.T. DeLand, G.E. Thomas, and J.J. Olivero, Long term variations in the frequency of polar mesospheric clouds in the Northern Hemisphere from SBUV, *Geophys. Res. Lett*., **36**, L02803, doi:10.1029/2008GL036048, 2009.

Siskind, D.E. and D.P. Drob, Use of NOGAPS-ALPHA as a bottom boundary for the NCAR/TIEGCM, AGU-Geophysical Monograph 201, Modeling the Ionosphere-Thermosphere System, pp. 171-180, 2014.

Siskind, D.E. *et al*., Consequences of recent Southern Hemisphere winter variability on polar mesospheric clouds, *J. Atm. Sol.-Terr. Phys*., **73**, 2013-2021, 2011.

Siskind, D.E. *et al*., Linkages between the cold summer mesopause and thermospheric zonal mean circulation, *Geophys. Res. Lett*., 39, L01804, doi: 10.1029/2011GL050196, 2012.

Siskind, D.E., D.P. Drob, K.F. Dymond and J.P. McCormack, Simulations of the effects of vertical transport on the thermosphere and ionosphere using two coupled models, *J. Geophys. Res*., **119**, 1172-1185, doi:10.1002/2013JA019116, 2014.

Stevens, M.H., C.R. Englert, M.T. DeLand, and M. Hervig, The polar mesospheric cloud mass in the Arctic summer, *J. Geophys. Res*., **110**, A02306, doi:10.1029/2004JA010566, 2005.

Stevens, M.H. *et al*. Tidally induced variations of polar mesospheric cloud altitudes and ice water content using a data assimilation system, *J. Geophys. Res*., **115**, D18209, doi:10.1029/2009JD013225, 2010.

Stevens, M.H. *et al*., Validation of upper mesospheric and lower thermospheric temperatures measured by the Solar Occultation for Ice Experiment, *J. Geophys. Res*., **117**, D16304, doi:10.1029/2012JD017689, 2012.

Stull, R.B., Meterology for Scientists and Engineers, second ed. Brooks/Cole, Pacific Grove, CA, 502 pp, 2000.

von Savigny, C., C. Robert, H. Bovensmann, J.P. Burrows, and M. Schwartz, Satellite observations of the quasi 5-day wave in noctilucent clouds and mesopause temperatures, *Geophys. Res. Lett*., **34**, L24808, doi:10.1029/2007GL030987, 2007.

Zhang, X. *et al*., Monthly tidal temperatures 20-120 km from TIMED/SABER, *J. Geophys. Res*., **111**, A10508, doi:10.1029/2005JA011504, 2006.